



ELSEVIER

doi:10.1016/j.gca.2004.12.022

Petrogenesis of Al-rich chondrules: Evidence from bulk compositions and phase equilibria

GLENN J. MACPHERSON,^{1,*} and GARY R. HUSS^{2,†}¹Department of Mineral Sciences, National Museum of Natural History, Smithsonian Institution, PO Box 37012, Washington, DC 20560-0119, USA²Department of Geology and Center for Meteorite Studies, Arizona State University, PO Box 871404, Tempe, AZ 85287-1404, USA

(Received January 23, 2003; accepted in revised form December 20, 2004)

Abstract—We measured major, minor, and trace-element compositions for eleven Al-rich chondrules from unequilibrated ordinary chondrites to investigate the relationships between Al-rich chondrules, ferromagnesian chondrules, Ca-, Al-rich inclusions (CAIs), and amoeboid olivine aggregates (AOAs). Phase equilibrium considerations show that, for the most part, mineral assemblages in Al-rich chondrules are those expected from melts of the observed compositions. The diversity of mineral assemblages and Al-rich chondrule types arises mainly from the fact that the array of compositions spans both the spinel-saturated anorthite-forsterite reaction curve and a thermal divide defined by where the anorthite-forsterite join crosses the reaction curve. The reaction curve accounts for the two principal varieties of Al-rich chondrule, plagioclase-phyric and olivine-phyric, with or without aluminous spinel. The thermal divide influences the subsequent evolution of each variety. A third variety of Al-rich chondrule contains abundant sodium-rich glass; trace-element fractionation patterns suggest that these glassy Al-rich chondrules could have been derived from the other two by extensive alteration of plagioclase to nepheline followed by remelting. The bulk compositions of Al-rich chondrules (except sodium-rich ones) are intermediate in a volatility sense between ferromagnesian chondrules and type C CAIs. The combined trend of bulk compositions for CAIs, Al-rich chondrules, and ferromagnesian chondrules mirrors, but does not exactly match, the trend predicted from equilibrium condensation at $P_T \sim 10^{-3}$ atm; the observed trend does not match the trend found for evaporation from a liquid of chondritic composition. We thus infer that the bulk compositions of the precursors to CAIs, Al-rich chondrules, were ferromagnesian chondrules were controlled primarily by vapor-solid reactions (condensation or sublimation) in the solar nebula. Some Al-rich chondrules are consistent with an origin by melting of a compound CAI-ferromagnesian chondrule hybrid; others cannot be so explained. Any hybrid model is restricted by the constraint that the CAI precursor consisted dominantly of pyroxene + plagioclase + spinel; melilite cannot have been a significant component. Amoeboid olivine aggregates also have the inferred mineralogical characteristics of Al-rich chondrule precursors—they are mixtures of olivine with plagioclase-spinel-pyroxene-rich CAIs—but the few measured bulk compositions are more olivine-rich than those of Al-rich chondrules. Copyright © 2005 Elsevier Ltd

1. INTRODUCTION

Chondrules and calcium-aluminum-rich inclusions (CAIs) are among the most ancient materials formed in our Solar System ~4.6 billion years ago. They are probes into the processes and conditions that existed in the solar nebula. Yet despite more than 30 years of detailed studies, the temporal and petrogenetic relationships between these two very different types of primitive objects are poorly understood. Did they form by similar or different processes, at different times or contemporaneously, and in the same or different localities? One approach to answering these questions is through the study of so-called Al-rich chondrules, which share mineralogical and chemical properties with both CAIs and ferromagnesian chondrules (informally, Fe-Mg rich and Al poor). Although Al-rich chondrules rarely have been studied in any systematic fashion (Bischoff and Keil, 1984; Sheng et al., 1991; Krot and Keil,

2002; Krot et al., 2002, 2004b), it is clear that in some way they must be petrogenetic links between ferromagnesian chondrules and CAIs. The importance of Al-rich chondrules is further enhanced by the fact that their constituent plagioclase feldspar and Al-rich glass have proven amenable to successful ion microprobe searches for radiogenic ^{26}Mg , the decay product of ^{26}Al ($t_{1/2} = 720,000$ y). This has allowed estimates to be made of the time duration between CAI formation and the onset of Al-rich (and at least some ferromagnesian) chondrule formation on the order of 1.5–2.5 million years (Kita et al., 2000; Huss et al., 2001).

This paper presents detailed bulk major and trace element chemical compositions of eleven chondrules that were analyzed as part of a comprehensive chemical and isotopic study of CAIs and Al-rich chondrules in unequilibrated ordinary chondrites (UOCs); they were selected on the basis of containing primary igneous phases with high Al/Mg ratios, suitable for Mg isotopic studies. When recast into normative components and plotted (along with literature data for similar chondrules) on relevant phase equilibrium diagrams, the great diversity of mineralogy and textures in the Al-rich chondrule population appear in general to be a direct and predictable result of the fact that their wide range of bulk compositions spans two major petrogenetic

* Author to whom correspondence should be addressed (glenn@volcano.si.edu).

† Current address: Hawaii Institute of Geophysics and Planetology, 1680 East-West Road, Post 602, University of Hawaii at Manoa, Honolulu, HI 96822 USA

boundaries: a reaction boundary curve and a thermal divide, both of which control the liquid line of descent of any individual chondrule. In addition, the bulk composition trend of Al-rich chondrules links the trends of Types IA/IB ferromagnesian chondrules and CAIs to form a single, highly nonlinear trend that appears to be controlled by the stoichiometry of solid mineral phases. This combined bulk composition trend approximately parallels, but does not exactly follow, the trend predicted by equilibrium condensation of a solar gas at low pressure. This result suggests that the three groups of objects are related by volatility-controlled processes involving vapor and solid. Finally, the normative components derived from bulk major element composition data commonly show correlations with trace element abundances. Preliminary reports on various aspects of this work were given by MacPherson and Russell (1997), Huss et al. (1997), and MacPherson and Huss (2000). Oxygen isotopic analyses of several of the Al-rich chondrules are given in Russell et al. (1997a, 1998, 2000); magnesium-isotopic results are reported in Russell et al. (1996, 1997b) and Huss et al. (2001).

2. METHODS AND SAMPLES

2.1. Chondrule Identification, Characterization, and Mineral Chemistry

Polished thin sections were examined by optical microscope and then studied using the Smithsonian's JEOL JSM-840A scanning electron microscope, which is equipped with a KeveX Si(Li) x-ray analyzer. Al-rich chondrules were located by systematically searching each entire thin section using x-ray area mapping.

Mineral major element compositions determined at the Smithsonian were measured using (through 1996) an ARL-SEM automated 9-spectrometer electron microprobe. Operating conditions were 15 kV accelerating voltage and 0.15 μA probe current. Data were reduced using the procedure of Bence and Albee (1968). Since 1997, a new JEOL JXA-8900R 5-spectrometer electron microprobe has been used for all mineral chemical analyses done at the Smithsonian. Operating conditions for this instrument were 15 kV accelerating voltage and 0.10–0.20 μA probe current. Data from this machine were corrected using a proprietary ZAF program. For both the ARL and JEOL instruments, natural and synthetic minerals were used as calibration standards. For glass and feldspar analyses on both machines, short counting times and a slightly defocused beam of $\sim 10\ \mu\text{m}$ were used to minimize sodium loss; on the JEOL instrument, decreased probe currents were employed as well for the same purpose.

Mineral major element compositions determined at Caltech were measured using a JEOL 733 automated 5-spectrometer electron microprobe. Operating conditions for mineral analyses were 15 kV accelerating voltage and 0.025 μA beam current. The electron beam was rastered over a $\sim 7.5 \times \sim 7.5\ \mu\text{m}$ area. For glass analyses, the beam current was reduced to 0.015 μA and the raster area was increased to $10 \times 10\ \mu\text{m}$. Natural and synthetic minerals were used for calibration. Data were corrected using the CITZAF program (Armstrong, 1995).

Between one and four analyses of trace-element abundances (not reported individually herein) were obtained for individual mineral phases to calculate bulk trace element compositions for the chondrules. They were determined with the Caltech PANURGE Cameca ims-3f ion probe, using an O^- primary ion beam. Energy filtering was used to suppress the signals of complex molecular interferences; for the rare earth elements (REE), measured signals were deconvolved into elemental and oxide components (Zinner and Crozaz, 1986; Fahey et al., 1987). Calcium was the reference element. Standards were synthetic Ti-pyroxene glass, Madagascar hibonite, HAL hibonite, and Aln δ (Sweden) perovskite.

2.2. Bulk Compositions

Bulk compositions for the Al-rich chondrules were calculated by combining modal mineral abundances for individual chondrules with

the average compositions (major, minor, and trace elements) of their constituent minerals. Modal mineral abundances were determined by point counting back-scattered electron images of the chondrules, in some cases manually and where possible by digital image analysis (pixel counting) using commercial software. We necessarily assumed that area fractions are equal to volume fractions. These were then converted into mass fractions using appropriate densities for the individual phases. For most phases there is little or no internal chemical variation within the minerals and simple arithmetic averages were used. Olivine in two chondrules and spinel in one show strong iron enrichment near rims and fractures that is believed to be a secondary (possibly parent body) effect; in these cases, only the magnesium-rich compositions were used. Plagioclase commonly is altered to nepheline. To calculate the primary bulk compositions, all modal nepheline was calculated as plagioclase. Glass in one chondrule showed significant variation and we used a simple average of all measurements.

One potentially significant source of error in determining bulk compositions by this method is that the slice through an object as exposed in the plane of the thin section may not be a representative sample of the object as a whole. This problem can arise from random fluctuations in modal mineralogy, but it will be most severe for off-center slices through objects whose interiors are systematically very different in mineralogy and chemistry from their outer regions, e.g., chondrules that possess spherically symmetric zoning in modal mineralogy. Even if the slice is reasonably believed to pass through the center of the chondrule, the relative areas of core and mantle still must be recalculated as concentric volumes in a sphere. For all but two of the chondrules studied here (Chainpur 1251-16-2 and 1251-3-1), the problems noted above do not appear to be significant (no evidence of zonation or other heterogeneity) and no correction was made. In Chainpur 1251-16-2 there is no way of knowing whether the modal relationship between the huge central olivine (see description below) and the minor surrounding enstatite-rich mesostasis is representative of the whole object. We were forced to accept the mode as measured, and no correction was made. Chainpur 1251-3-1 is concentrically zoned, with most of the diopside and spinel concentrated in the chondrule core and most of the glass, metal, and sulfide in its outer regions. There is no way of determining if the plane of the section goes through the center of the chondrule in such a small object, so we necessarily assumed that it does. We used digital image analysis to measure the separate modes in the core and mantle, and then calculated their relative spherical volumes.

2.3. Petrography and Mineral Chemistry of the Al-Rich Chondrules

Modal mineral abundances for the Al-rich chondrules are given in Table 1. Compositions of individual phases are given in Tables 2–6. Partial descriptions of some of these chondrules were published previously, but we include complete descriptions of all here to provide a basis for later discussions.

Chainpur 1251-16-2 (Fig. 1a) is an ovoid and complex chondrule or chondrule fragment, $\sim 600 \times \sim 700\ \mu\text{m}$ in size. The chondrule is dominated by one large, severely scalloped and corroded olivine crystal that is zoned from Fo_{93} in its core to Fo_{82} along fractures and at its edges (Table 2). External to the olivine is a discontinuous outer zone consisting of untwinned enstatite crystals (En_{92} , Table 5) that locally enclose round blebs of Fe-rich olivine (Fo_{67-71}). Enclosed within the core of the olivine crystal, which is also the center of the chondrule, is a large irregular area consisting of enstatite, zoned olivine grains, and interstitial plagioclase (An_{79} , Table 4) and diopside (Table 5); minor nepheline partially replaces plagioclase. The core may be a trapped relict fragment or else a plagioclase-rich re-entrant of the enstatite rim zone that projects into the olivine from the third dimension. The inferred order of appearance of phases in this "relict" core is olivine, enstatite, and diopside + plagioclase.

Krymka 1729-9-1 (Fig. 1b) is a rounded chondrule $\sim 1\ \text{mm}$ in diameter, truncated on one side by the thin section edge. It has a granular texture, consisting mostly of blocky olivine grains (Fo_{83-85} , Table 2) with interstitial anhedral plagioclase (An_{85-87} , Table 4). In the interior of the chondrule are rare grains of metal (5.7% Ni), pigeonite that has exsolved to enstatite and augite (Table 5) as well as ilmenite (avg. $\sim 3.6\%$ MgO). Small enstatite grains (Table 5) occur around the periphery of the chon-

Table 1.: Modal abundances in Al-rich chondrules (reported in weight percentages¹; errors 2σ from counting statistics).

	Chainpur 1251-16-2	Krymka 1729-9-1	Quinyambie ² 6076-5-2	Chainpur 1251-14-1	Inman ³ 5652-1-1	Semarkona 4128-3-2	Chainpur 5674-2-1	Chainpur 1251-14-2	Chainpur 5674-3b-1	Chainpur 1251-16-3	Chainpur ⁴ 1251-3-1
Plagioclase	5.8 ± 0.9	17.4 ± 3.0	32.7 ± 3.7	26.6 ± 3.0	30.0 ± 0.3	36.5 ± 5.1	41.7 ± 4.4	46.8 ± 2.8	17.1 ± 2.5	26.9 ± 2.5	62.0 ± 0.5
Al-rich Glass						2.6 ± 1.4				0.9 ± 0.5 ⁵	22.9 ± 0.4
Pyroxene High-Ca	5.6 ± 0.9	0.3 ± 0.4		25.9 ± 3.3	23.3 ± 0.2	9.2 ± 2.8	29.4 ± 4.0	42.5 ± 2.9			
Low-Ca	24.6 ± 2.8	15.3 ± 3.0	37.1 ± 4.2								
Pigeonite		trace									
Olivine	61.0 ± 6.5	66.8 ± 6.3	30.2 ± 3.8	38.6 ± 3.9	43.5 ± 0.3	45.7 ± 6.1	14.6 ± 2.8		57.1 ± 5.4	42.7 ± 3.6	10.4 ± 0.2
Spinel				5.8 ± 1.6	3.2 ± 0.9	5.5 ± 2.3					3.1 ± 0.1
Fe-Ni Metal	0.5 ± 0.3	<0.1 ± 0.3		2.3 ± 1.5		0.6 ± 1.1			16.1 ± 3.7	21.8 ± 4.1	1.1 ± 0.1
Troilite	0.3 ± 0.2			0.7 ± 0.7					9.7 ± 2.3	7.7 ± 1.9	0.4 ± 0.1
Nepheline	2.2 ± 0.5										
Ilmenite		0.2 ± 0.5					14.2 ± 2.5	10.7 ± 1.3			
Total points	1196	692	874	1012	166716 ⁶	514	809	2227	890	1219	88273 ⁶

¹ Volume percentages were converted to weight percentages using mineral densities from Beckett (1986) and Deer, Howie, and Zussman (1966).

² Maskelynite included in plagioclase abundance.

³ Mode of barred portion of chondrule—brecciated portion not included (see text).

⁴ Mode of this zoned chondrule calculated assuming the inner “core” and outer “mantle” make up 33 and 67 volume percent, respectively, of a concentrically zoned sphere.

⁵ Combined abundance for all pyroxenes; they are to intimately inter-grown for independent abundances (see text and Fig. 1).

⁶ Pixels; mode measured using digital image analysis.

drule, rimming olivine. It is reasonably clear that olivine was the first crystallizing phase, but textures relevant to the rest of the crystallization sequence are ambiguous. For the silicates, the best estimate is olivine, followed by plagioclase or enstatite, and finally pigeonite.

Quinyambie 6076-5-2 (Fig. 1 of Russell et al., 2000) is a rounded chondrule at least 575 μm in diameter, but possibly larger because half or more of the chondrule is truncated by the edge of the thin section. This chondrule was first described by Russell et al. (1996) and labeled Moorabie 6076-5-2 because at the time the two meteorites were believed to be paired. It is composed of blocky olivine crystals up to ~130 μm in size (Fo₈₂₋₈₄, Table 2) that are partially mantled by Mg-rich, subcalcic augite (Table 5). Interstitial to these are anhedral, partly maskelynitized plagioclase crystals (~An₆₆₋₈₃, Table 4) up to ~100 μm in length. The olivines are, in places, mantled directly by plagioclase without intervening pyroxene. Thus plagioclase may have preceded pyroxene in the crystallization sequence. Accordingly, the texturally inferred crystallization sequence is olivine, then plagioclase, and finally pyroxene.

Chainpur 1251-14-1 is a slightly elliptical chondrule, just under 600 μm in maximum dimension, which was described by Russell et al. (1996) (their Fig. 1b). It is porphyritic, with abundant euhedral phenocrysts (≲85 μm) of olivine (Fo₉₆₋₉₉, Table 2) and sparse euhedral spinels (FeO = 1%, Table 3; most <30 μm, but one central crystal is 185 μm) set in a finer-grained groundmass of euhedral to somewhat skeletal plagioclase laths (An₈₆₋₈₉, Table 4), ophitic aluminous diopside (Table 5), and sparse troilite and iron-nickel metal beads. Some spinel grains are enclosed within forsterite, suggesting that spinel preceded olivine in the crystallization sequence. Plagioclase laths are without exception truncated where they abut forsterite and spinel. Near the outermost margin of the chondrule the olivine and spinel crystals show minor enrichment in FeO (e.g., Table 4) along crystal edges and fractures. The inferred order of appearance of crystallizing phases is spinel, olivine, plagioclase, and then pyroxene.

Inman 5652-1-1 is a complex predominantly barred olivine chondrule that was described by Russell et al. (1996) (their Fig. 1d). Its original size is somewhat uncertain because the thin section edge truncates it, but we estimate the diameter of this rounded object to be just over 500 μm. Throughout most of the chondrule, skeletal olivine bars (Fo₉₄₋₉₉, Table 2) cut across laths of anorthite (An₉₅₋₉₉, Table 4) that are locally subparallel to one another and nearly perpendicular to the olivine, giving this portion of the chondrule a cross-banded texture. Interstitial to the feldspar is aluminous diopside (Table 5). Rare corroded spinel grains (e.g., Table 4) are enclosed in olivine and plagioclase. One end of the chondrule is fragmented, contains far less olivine than the main portion, and the barred texture is missing. Thus Inman 5652-1-1 appears to be a compound chondrule. The olivine-poor region is laced with veins of terrestrial Fe oxide that also permeate much of the meteorite in general. Around the periphery of much of the entire chondrule is a fine-grained 10–20-μm-thick rim that consists of small (<5 μm) rounded blebs of olivine enclosed within pyroxene; the pyroxene is distinctly poorer in Al and Ti relative to the interior pyroxene (Table 5). Excluding the rim and based on the barred olivine region only, the texturally inferred order of crystallization is spinel first, followed by olivine, plagioclase, and finally pyroxene. All subsequent discussion of this chondrule will refer to the barred portion only.

Semarkona 4128-3-2 (Fig. 1c) is a lens-shaped chondrule fragment, 350 × 310 μm, with a partly developed barred-olivine structure. Interstitial to the olivine bars (Fo₉₉₋₁₀₀, Table 2) are ~40 × ~10 μm laths and hopper-shaped crystals of untwinned calcic plagioclase (containing 6%–8% of the magnesium plagioclase component,* CaMgSi₃O₈; Table 4; see Longhi et al., 1976), small blocky grains of aluminous diopside (Table 5), and minor SiO₂-rich glass. Near the center of the chondrule is a single ~50-μm equant crystal of spinel (Table 3). The crystallization sequence inferred from textures is some-

* The high Mg is very reproducible, and measurements on widely separated dates using two different microprobes were indistinguishable. Analyses contaminated by beam overlap onto neighboring olivine and pyroxene were easily recognized and thus eliminated from consideration on the basis of Mg vs Si stoichiometry diagrams, and only superior analyses were used in arriving at the average analysis given in Table 4.

Table 2. Average composition of olivine in Al-rich chondrules.¹

Chondrule	Chainpur 1251-16-2				
	Chainpur 1251-16-2 Mg-Rich (N = 3)	Intermediate (N = 9 ²)	Chainpur 1251-16-2 Fe-Rich (N = 2)	Krymka 1729-9-1 (N = 10)	Quinyambie 6076-5-2 (N = 9)
SiO ₂	40.9 ± 0.5	39.9 ± 1.2	37.7 ± 1.2	39.4 ± 0.7	39.2 ± 0.6
TiO ₂	0.09 ± 0.5	0.08 ± 0.03	0.035 ± 0.007	0.05 ± 0.06	0.04 ± 0.02
Al ₂ O ₃	0.00 ± 0.00	0.03 ± 0.09	0.08 ± 0.20	0.05 ± 0.09	0.1 ± 0.2
Cr ₂ O ₃	0.061 ± 0.007	0.07 ± 0.03	0.3 ± 0.7	ND	ND
FeO	7.8 ± 1.1	13.9 ± 3.9	26.0 ± 5.9	15.9 ± 1.2	16.2 ± 1.4
MnO	ND	0.14	0.37 ± 0.03	ND	ND
V ₂ O ₃	ND	0.004	0.02 ± 0.05	0.000 ± 0.003	0.002 ± 0.005
NiO	ND	0.04	0.00 ± 0.00	ND	ND
MgO	50.7 ± 0.5	45.3 ± 2.9	34.6 ± 3.2	45.1 ± 1.3	43.3 ± 0.5
CaO	0.17 ± 0.04	0.12 ± 0.14	0.14 ± 0.17	0.24 ± 0.07	0.27 ± 0.05
Na ₂ O	0.00 ± 0.00	0.002 ± 0.010	0.01 ± 0.03	0.01 ± 0.02	0.009 ± 0.018
K ₂ O	0.003 ± 0.005	0.006 ± 0.013	0.001 ± 0.004	0.002 ± 0.007	0.00 ± 0.012
Total	99.72	99.59	99.26	100.75	99.13
Fo range	91-93	82-88	67-71	83-85	82-84

Chondrule	Chainpur 1251-14-1				
	Chainpur 1251-14-1 (N = 9)	Inman 5652-1-1 (N = 10)	Semarkona 4128-3-2 (N = 5)	Chainpur 5674-2-1 Mg-Rich (N = 7)	Chainpur 5674-2-1 Fe-Rich (N = 2)
SiO ₂	41.7 ± 1.0	41.5 ± 1.7	41.8 ± 1.1	41.5 ± 1.0	36.6 ± 1.5
TiO ₂	0.09 ± 0.05	0.09 ± 0.03	0.06 ± 0.04	0.08 ± 0.10	0.11 ± 0.02
Al ₂ O ₃	0.19 ± 0.19	0.5 ± 0.3	0.11 ± 0.12	0.2 ± 0.4	0.07 ± 0.02
Cr ₂ O ₃	0.13 ± 0.07	ND	0.24 ± 0.16	0.13 ± 0.19	ND
FeO	1.2 ± 2.6	2.5 ± 2.5	0.5 ± 0.3	4.8 ± 3.5	28.5 ± 2.8
MnO	0.03 ± 0.04	ND	0.14 ± 0.19	ND	ND
V ₂ O ₃	0.04 ± 0.05	0.02 ± 0.03	0.039 ± 0.006	ND	ND
NiO	0.05 ± 0.09	ND	ND	ND	ND
MgO	54.7 ± 1.7	55.2 ± 2.7	56.6 ± 1.0	52.9 ± 2.5	32.6 ± 2.0
CaO	0.6 ± 0.5	0.56 ± 0.07	0.35 ± 0.03	0.41 ± 0.11	0.48 ± 0.04
Na ₂ O	0.02 ± 0.02	0.004 ± 0.008	0.008 ± 0.015	0.04 ± 0.05	0.013 ± 0.010
K ₂ O	0.002 ± 0.011	0.000 ± 0.001	0.007 ± 0.013	0.004 ± 0.014	0.002 ± 0.003
Total	98.75	100.37	99.85	100.06	98.38
Fo range	96-99	94-99	99-100	92-99	60-68

Chondrule	Chainpur 5674-3b-1		
	Chainpur 5674-3b-1 (N = 17)	Chainpur 1251-16-3 (N = 18)	Chainpur 1251-3-1 (N = 13)
SiO ₂	42.1 ± 0.6	41.9 ± 1.2	41.8 ± 0.8
TiO ₂	0.05 ± 0.03	0.05 ± 0.05	0.06 ± 0.10
Al ₂ O ₃	0.09 ± 0.08	0.04 ± 0.06	0.09 ± 0.12
Cr ₂ O ₃	0.08 ± 0.04	0.10 ± 0.11	0.08 ± 0.04
FeO	2.4 ± 2.3	3.7 ± 5.3	0.4 ± 0.06
MnO	0.03 ± 0.03	0.07 ± 0.03	0.01 ± 0.02
V ₂ O ₃	0.007 ± 0.009	0.003 ± 0.013	0.02 ± 0.04
NiO	ND	0.01 ± 0.05	0.01 ± 0.05
MgO	54.7 ± 2.1	54.3 ± 4.6	56.2 ± 0.8
CaO	0.34 ± 0.06	0.21 ± 0.03	0.30 ± 0.12
Na ₂ O	0.007 ± 0.006	0.003 ± 0.008	0.01 ± 0.04
K ₂ O	0.006 ± 0.004	0.007 ± 0.013	0.015 ± 0.015
Total	99.81	100.39	99.00
Fo range	91-99	90-99	99-100

ND = Not Determined

¹ Reported in wt. %. Errors are 2σ standard deviations of individual measurements.² Mean for MnO, V₂O₃, and NiO in Chainpur 1251-16-2 intermediate olivine comes from a single measurement.

what ambiguous: spinel + olivine (relative order unclear) appeared first, followed by anorthite + pyroxene (with residual glass).

Chainpur 5674-2-1 (Fig. 1d) is a slightly elliptical chondrule, 440 × 500 μm, whose texture is dominated by large euhedral anorthite laths (An₉₀₋₉₈, Table 4) up to 350 μm long and 65 μm wide (Fig. 2c). The cores of the largest laths have been mostly replaced by nepheline. Accompanying the plagioclase are sparse blocky olivine grains (interior: Fo₉₂₋₉₉, Table 2), some with hollow cores, which in a few cases appear to be partly enclosed within the end or edges of large plagioclase crystals. Clearly interstitial to both the olivine and plagioclase are blocky to branching aluminous diopside (Table 5) and fine dendritic

intergrowths consisting variously of olivine + plagioclase and diopside + plagioclase. The interstitial plagioclase is slightly more sodic in composition (An₈₃₋₈₈, Table 4) than the phenocrysts. There is a small amount of residual glass. Near the exterior of the chondrule, the olivine crystals are Fe-rich (Fo₆₀, Table 2) along grain margins and fractures. Plagioclase and olivine were the earliest crystallizing phases, but their relative order is ambiguous. The observation that olivine is not found in the middle of the largest plagioclase laths hints that anorthite appeared first, followed closely by olivine, and then finally pyroxene.

Chainpur 1251-14-2 (Fig. 1e) is an irregularly shaped chondrule, ~300 μm in maximum dimension. It is composed mainly of large

Table 3. Average composition of spinel in Al-rich chondrules.¹

Chondrule	Chainpur 1251-14-1 Mg-Rich (N = 2)	Chainpur 1251-14-1 Fe-Rich (N = 6)	Inman 5652-1-1 (N = 1)	Semarkona 4128-3-2 (N = 6 ²)	Chainpur 1251-3-1 (N = 12)
SiO ₂	0.08 ± 0.02	0.17 ± 0.15	1.27	0.11 ± 0.08	0.04 ± 0.04
TiO ₂	0.32 ± 0.04	0.40 ± 0.16	0.31	0.26 ± 0.03	0.28 ± 0.11
Al ₂ O ₃	69.6 ± 2.0	68.8 ± 2.6	64.4	69.5 ± 0.6	70.7 ± 0.5
Cr ₂ O ₃	0.323 ± 0.011	0.5 ± 0.5	3.79	0.64 ± 0.14	0.17 ± 0.07
FeO	0.6 ± 0.3	3.7 ± 4.7	5.92	0.30 ± 0.03	0.8 ± 0.7
MnO	0.02 ± 0.02	0.03 ± 0.02	0.09	0.014	0.01 ± 0.02
V ₂ O ₃	0.34 ± 0.04	0.31 ± 0.13	0.09	0.31	0.25 ± 0.04
NiO	0.04 ± 0.03	0.05 ± 0.09	0.07	ND	0.02 ± 0.06
MgO	27.7 ± 0.4	25.9 ± 3.4	23.8	28.8 ± 0.5	27.7 ± 1.3
CaO	0.028 ± 0.009	0.06 ± 0.05	0.31	0.044 ± 0.019	0.02 ± 0.03
Na ₂ O	0.02 ± 0.02	0.01 ± 0.02	0.02	0.004 ± 0.004	0.005 ± 0.018
K ₂ O	0.000 ± 0.000	0.000 ± 0.000	0.00	0.008 ± 0.019	0.01 ± 0.02
Total	99.07	99.93	100.07	99.99	100.01

ND = Not Determined.

¹ Reported in wt. %. Errors are 2σ standard deviations of individual measurements.

² Only one of six measurements included MnO and V₂O₃.

plagioclase laths up to ~185 μm long (An₈₉₋₉₇, Table 4), which are partially replaced by nepheline. Interstitial to the feldspar laths is a blocky to dendritic intergrowth of plagioclase and aluminous diopside (Table 5). The plagioclase is unusual in two respects: It is riddled with

submicron-sized round holes, and the polysynthetic twinning plane is oriented ~60° away from the length of the crystals. The pyroxene is the most aluminum-rich of any of the chondrules we studied, and the composition is bimodal in terms of aluminum. This suggests that the

Table 4. Average composition of plagioclase in Al-rich chondrules.¹

Chondrule	Chainpur 1251-16-2 (N = 3)	Chainpur 1251-14-2 (N = 39)	Krymka 1729-9-1 (N = 14)	Quinyambie 6076-5-2 ² (N = 12)	Chainpur 1251-14-1 (N = 7)
SiO ₂	48.2 ± 0.5	44.7 ± 1.4	46.3 ± 0.8	46.1 ± 1.3	45.6 ± 1.0
TiO ₂	0.08 ± 0.09	0.2 ± 0.2	0.02 ± 0.02	0.07 ± 0.04	0.12 ± 0.03
Al ₂ O ₃	33.35 ± 0.18	35.3 ± 1.3	33.6 ± 0.6	33.3 ± 1.1	34.6 ± 0.6
Cr ₂ O ₃	0.025 ± 0.001	0.008 ± 0.015	0.010 ± 0.016	0.02 ± 0.03	0.03 ± 0.03
FeO	0.45 ± 0.07	0.2 ± 0.2	0.7 ± 0.2	0.9 ± 0.7	0.5 ± 0.4
MnO	0.03 ± 0.07	ND	ND	0.03 ± 0.04	0.02 ± 0.02
V ₂ O ₃	0.02 ± 0.13	0.01 ± 0.03	0.004 ± 0.008	0.02 ± 0.02	0.01 ± 0.04
NiO	0.003 ± 0.004	ND	ND	0.04 ± 0.10	0.05 ± 0.13
MgO	0.33 ± 0.08	0.2 ± 0.4	0.64 ± 0.16	0.6 ± 0.3	0.4 ± 0.4
CaO	16.21 ± 0.16	18.9 ± 1.0	18.1 ± 0.3	14.9 ± 2.3	17.5 ± 0.4
Na ₂ O	2.49 ± 0.13	0.8 ± 0.5	1.35 ± 0.17	3.8 ± 2.1	1.6 ± 0.3
K ₂ O	0.041 ± 0.014	0.02 ± 0.04	0.008 ± 0.010	0.2 ± 0.4	0.04 ± 0.04
Total	101.23	100.34	100.73	99.98	100.47
An range	79	89-97	85-87	66-83	86-89

Chondrule	Inman 5652-1-1 (N = 30)	Semarkona 4128-3-2 (N = 16)	Chainpur 5674-2-1 Anorthite (N = 53)	Chainpur 5674-2-1 Bytownite (N = 12)
SiO ₂	44.0 ± 0.9	48.0 ± 1.3	44.1 ± 0.8	46.5 ± 1.1
TiO ₂	0.06 ± 0.04	0.16 ± 0.28	0.08 ± 0.09	0.08 ± 0.05
Al ₂ O ₃	35.6 ± 0.8	30.7 ± 2.5	35.6 ± 0.7	34.2 ± 1.1
Cr ₂ O ₃	0.004 ± 0.009	0.03 ± 0.07	0.007 ± 0.015	0.007 ± 0.017
FeO	0.3 ± 0.3	0.2 ± 0.3	0.27 ± 0.16	0.32 ± 0.15
MnO	ND	0.03 ± 0.03	ND	ND
V ₂ O ₃	0.007 ± 0.013	0.008 ± 0.009	0.002 ± 0.008	0.004 ± 0.009
NiO	ND	0.010 ± 0.028	ND	ND
MgO	0.5 ± 0.2	1.9 ± 1.5	0.3 ± 0.3	0.21 ± 0.19
CaO	20.1 ± 0.5	18.4 ± 1.0	19.4 ± 0.6	17.5 ± 0.8
Na ₂ O	0.07 ± 0.06	0.42 ± 0.19	0.5 ± 0.4	1.6 ± 0.4
K ₂ O	0.004 ± 0.010	0.02 ± 0.02	0.008 ± 0.018	0.02 ± 0.03
Total	100.65	99.88	100.27	100.44
An range	95-99	80-86	90-98	83-88

ND = Not Determined.

¹ Reported in wt. %. Errors are 2σ standard deviations of individual measurements.

² Maskelynite-composition is non-stoichiometric. Original plagioclase may have been more anorthitic.

Table 5. Average composition of pyroxene in Al-rich chondrules.¹

Chondrule	Chainpur 1251-16-2	Chainpur 1251-16-2	Krymka 1729-9-1	Krymka 1729-9-1	Quinyambie 6076-5-2
	Diopside (N = 2)	Enstatite (N = 19)	Augite (N = 9)	Enstatite (N = 7)	Sub-Ca Augite (N = 7)
SiO ₂	54.0 ± 0.5	57.4 ± 0.9	51.2 ± 2.7	54.6 ± 0.2	53.0 ± 3.0
TiO ₂	0.9 ± 0.6	0.33 ± 0.20	2.4 ± 1.2	0.16 ± 0.03	0.40 ± 0.06
Al ₂ O ₃	4.2 ± 0.3	2.2 ± 1.0	3.8 ± 1.3	1.97 ± 0.11	3.7 ± 1.2
Cr ₂ O ₃	1.44 ± 0.07	1.2 ± 0.3	1.2 ± 0.3	1.36 ± 0.08	ND
FeO	2.0 ± 0.6	3.8 ± 2.2	6.9 ± 2.5	10.5 ± 0.3	10.9 ± 0.3
MnO	0.089 ± 0.007	0.20 ± 0.23	ND	0.29 ± 0.07	ND
V ₂ O ₃	0.06 ± 0.07	0.04 ± 0.03	0.010 ± 0.014	0.05 ± 0.03	0.03 ± 0.03
NiO	0.03 ± 0.08	0.004 ± 0.008	ND	0.05 ± 0.06	ND
MgO	20.4 ± 1.5	34.0 ± 1.6	18.3 ± 5.0	29.7 ± 0.3	22.8 ± 2.1
CaO	19.0 ± 1.6	2.3 ± 0.9	16.5 ± 6.7	1.78 ± 0.14	8.7 ± 1.4
Na ₂ O	0.022 ± 0.014	0.006 ± 0.016	0.01 ± 0.03	0.04 ± 0.04	0.07 ± 0.08
K ₂ O	0.004 ± 0.011	0.005 ± 0.008	0.010 ± 0.013	0.010 ± 0.016	0.03 ± 0.04
Total	102.15	101.49	100.33	100.51	99.63

Chondrule	Chainpur 1251-14-1	Inman 5652-1-1	Inman 5652-1-1	Semarkona 4128-3-2	Chainpur 5674-2-1
	(N = 21)	Al-Diopside (N = 16)	Diopside (N = 5)	Al-Diopside (N = 6)	Diopside (N = 9)
SiO ₂	46.7 ± 2.5	45.4 ± 1.5	51.4 ± 0.6	52.7 ± 0.3	47.5 ± 0.7
TiO ₂	2.3 ± 1.0	2.5 ± 1.0	1.25 ± 0.19	2.00 ± 0.17	3.8 ± 1.1
Al ₂ O ₃	11.9 ± 2.6	13.9 ± 2.6	4.3 ± 1.2	5.8 ± 1.0	8.4 ± 0.9
Cr ₂ O ₃	0.44 ± 0.14	0.7 ± 0.6	1.02 ± 0.14	0.84 ± 0.09	0.7 ± 0.6
FeO	0.3 ± 0.6	2.3 ± 1.8	3.9 ± 1.2	0.45 ± 0.14	0.17 ± 0.04
MnO	0.05 ± 0.03	ND	ND	0.41 ± 0.10	0.03 ± 0.03
V ₂ O ₃	0.02 ± 0.04	0.01 ± 0.03	0.010 ± 0.009	0.031 ± 0.011	0.03 ± 0.04
NiO	0.05 ± 0.10	ND	ND	0.03 ± 0.03	0.02 ± 0.05
MgO	14.4 ± 1.7	12.5 ± 1.5	18.4 ± 2.0	18.4 ± 0.9	15.5 ± 0.8
CaO	24.3 ± 1.5	23.7 ± 2.6	20.2 ± 1.2	18.5 ± 1.1	22.5 ± 0.4
Na ₂ O	0.03 ± 0.06	0.008 ± 0.022	0.002 ± 0.006	0.12 ± 0.07	0.04 ± 0.07
K ₂ O	0.011 ± 0.019	0.004 ± 0.012	0.007 ± 0.010	0.010 ± 0.015	0.01 ± 0.02
Total	100.50	101.39	100.49	99.29	98.70

Chondrule	Chainpur 1251-14-2	Chainpur 1251-14-2	Chainpur 1251-16-3	Chainpur 1251-16-3	Chainpur 1251-3-1
	Al-Diopside (N = 3)	Al-Diopside (N = 4)	Al-Diopside (N = 4)	Pigeonite (N = 1)	Al-Diopside (N = 12)
SiO ₂	50.0 ± 1.4	40.7 ± 0.9	51.6 ± 2.3	58.5	47.8 ± 3.0
TiO ₂	2.0 ± 0.5	3.2 ± 0.5	1.83 ± 0.14	0.53	1.6 ± 1.2
Al ₂ O ₃	8.3 ± 1.0	23.1 ± 1.8	8.2 ± 1.9	2.6	12.7 ± 4.8
Cr ₂ O ₃	0.04 ± 0.03	0.05 ± 0.04	0.69 ± 0.03	0.54	0.21 ± 0.15
FeO	0.25 ± 0.16	0.3 ± 0.7	1.1 ± 2.1	0.53	0.16 ± 0.07
MnO	0.01 ± 0.03	0.04 ± 0.03	0.125 ± 0.001	0.12	0.04 ± 0.04
V ₂ O ₃	0.01 ± 0.04	0.02 ± 0.04	0.02 ± 0.04	0.015	0.01 ± 0.03
NiO	0.08 ± 0.24	0.07 ± 0.11	0.10 ± 0.15	0.077	0.02 ± 0.05
MgO	16.6 ± 0.5	10.4 ± 1.4	21.0 ± 3.3	36.0	17.5 ± 3.1
CaO	22.1 ± 0.5	22.6 ± 1.1	16.7 ± 2.6	2.9	19.3 ± 4.4
Na ₂ O	0.07 ± 0.13	0.14 ± 0.28	0.08 ± 0.19	0.02	0.10 ± 0.20
K ₂ O	0.022 ± 0.005	0.03 ± 0.07	0.04 ± 0.05	0.02	0.04 ± 0.04
Total	99.48	100.65	101.49	101.85	99.48

ND = Not Determined.

¹ Reported in wt. %. Errors are 2σ standard deviations of individual measurements.

pyroxene is sector zoned. The textures indicate that plagioclase was the liquidus phase, followed by pyroxene.

Chainpur 5674-3b-1 (Fig. 1f) is a subrounded, compound chondrule ~850 μm in diameter. Most of the object has a porphyritic-olivine texture consisting of a densely packed array of equant euhedral to subhedral olivine crystals and abundant rounded metal and sulfide blebs imbedded in clear pink isotropic glass. Metal and sulfide shapes are subordinate to those of olivine, suggesting the latter solidified first. This porphyritic region encloses what appears to be half of a barred-olivine chondrule that was originally ~400 μm in maximum dimension. The barred region contains a single set of olivine bars 20–25 μm thick in optical continuity with a discontinuous olivine shell of about the same thickness that mantles the

round surface of the hemispherical chondrule. Interstitial to the olivine bars is clear pink isotropic glass. Unlike the enclosing porphyritic portion, the barred region is nearly metal and sulfide free. Both the granular and the barred olivine crystals are very Mg rich (Fo_{98–99}); only very thin crystal margins and areas bordering fractures are more Fe rich (Fo₉₁, Table 2). Glass in the barred region is somewhat poorer in SiO₂ and MgO, and richer in Al₂O₃ and Na₂O, than that in the porphyritic region (Table 6).

Chainpur 1251-16-3 (Fig. 1g) is a round barred-olivine chondrule (diameter ~450 μm) with two sets of Mg-rich olivine bars (Fo_{90–99}, Table 2) intersecting at ~50°, set in clear pink isotropic glass (Table 6). The more Fe-rich olivine compositions are confined to thin zones along crystal margins and along fractures and cleavage traces in

Table 6. Average compositions of sodium-rich glasses in Al-rich chondrules.¹

Chondrule	Semarkona 4128-3-2 N = 1 ²	Chainpur 5674-3b-1 Barred Region (N = 4)	Chainpur 5674-3b-1 Porph. Region (N = 2)	Chainpur 5674-3b-1 All Glass (N = 6)	Chainpur 1251-16-3 (N = 9)	Chainpur 1251-3-1 (N = 27)
SiO ₂	65.21	52.6 ± 2.8	61.3 ± 7.1	55.5 ± 9.7	60.9 ± 2.9	58.6 ± 3.6
TiO ₂	1.47	1.1 ± 0.3	0.81 ± 0.03	1.0 ± 0.4	1.0 ± 0.3	1.1 ± 0.3
Al ₂ O ₃	11.51	27.7 ± 1.8	21.6 ± 4.7	25.7 ± 6.8	21.6 ± 1.3	23.1 ± 2.7
Cr ₂ O ₃	0.43	0.23 ± 0.05	0.11 ± 0.02	0.19 ± 0.12	0.51 ± 0.13	0.12 ± 0.10
FeO	0.19	1.7 ± 0.8	1.52 ± 0.04	1.6 ± 0.6	1.6 ± 0.3	1.4 ± 0.3
MnO	0.30	0.03 ± 0.04	0.03 ± 0.09	0.03 ± 0.05	0.01 ± 0.03	0.02 ± 0.05
V ₂ O ₃	0.007	0.008 ± 0.009	0.001 ± 0.003	0.006 ± 0.010	0.002 ± 0.010	0.005 ± 0.020
NiO	0.004	0.006 ± 0.014	0.06 ± 0.02	0.02 ± 0.05	0.03 ± 0.06	0.04 ± 0.08
MgO	4.71	0.13 ± 0.08	0.6 ± 0.6	0.3 ± 0.6	0.3 ± 0.2	0.5 ± 0.3
CaO	10.58	0.11 ± 0.03	0.04 ± 0.03	0.09 ± 0.07	0.04 ± 0.02	0.08 ± 0.03
Na ₂ O	2.95	15.5 ± 1.0	12.3 ± 2.6	14.4 ± 3.6	12.8 ± 0.9	13.3 ± 1.7
K ₂ O	0.50	1.22 ± 0.07	1.8 ± 0.3	1.4 ± 0.6	1.80 ± 0.18	1.7 ± 0.3
Total	97.85	100.31	100.17	100.24	100.59	99.99

¹ Reported in wt. %. Errors are 2 σ standard deviations of individual measurements.

² Most or all of our analyses of glass in this chondrule are contaminated by adjacent phases. This is the analysis that is least contaminated.

the crystals; the primary olivine composition is therefore interpreted to be highly Mg-rich. At the chondrule margin is a discontinuous 25–50- μ m-thick shell of coarse olivine, parts of which are in optical continuity with the internal bars. A few small skeletal pyroxene crystals up to ~40 μ m across occur in the glass. They consist of pigeonite cores rimmed by aluminous diopside (Table 5); very thin exsolution lamellae are present in the pigeonite. A large metal-troilite nodule is located on one edge of the chondrule, and small (~10 μ m) metal spheres are enclosed in the olivine shell. A partial rim of fine-grained troilite is present where the metal-troilite nodule contacts the matrix. The crystallization sequence of the silicates is inferred to be olivine followed by pigeonite, then diopside.

Chainpur 1251-3-1 is a broken, originally spherical, chondrule ~850 μ m in maximum dimension (described in Russell et al., 1996; their Fig. 1c). It is porphyritic, with stubby and somewhat rounded spinel crystals (Table 3; up to ~125 μ m) and elongate skeletal olivine crystals (Fo_{99–100}; Table 2; up to ~290 μ m) set in a mesostasis of dendritic aluminous diopside (Table 5) and Na-rich glass (Table 6). In the few places where the two phases are in contact, olivine partially encloses the spinel crystals. Diopside is everywhere subordinate in shape to olivine and spinel. Decorating the outermost edge of the chondrule are numerous small blocky pyroxene crystals that clearly nucleated there and grew inward; unlike the diopside in the center of the chondrule, these exterior diopside crystals have cores of pigeonite (Table 5). A few small blebs of metal and troilite also occur near the margin of the chondrule. Based on these relationships, a reasonable estimate of the order of appearance of phases is spinel and olivine followed by pigeonite, and lastly diopside. However, the spinel may be xenocrystic (see below).

3. RESULTS

3.1. Petrographic Summary, Major Element Bulk Chemistry, and Correlations

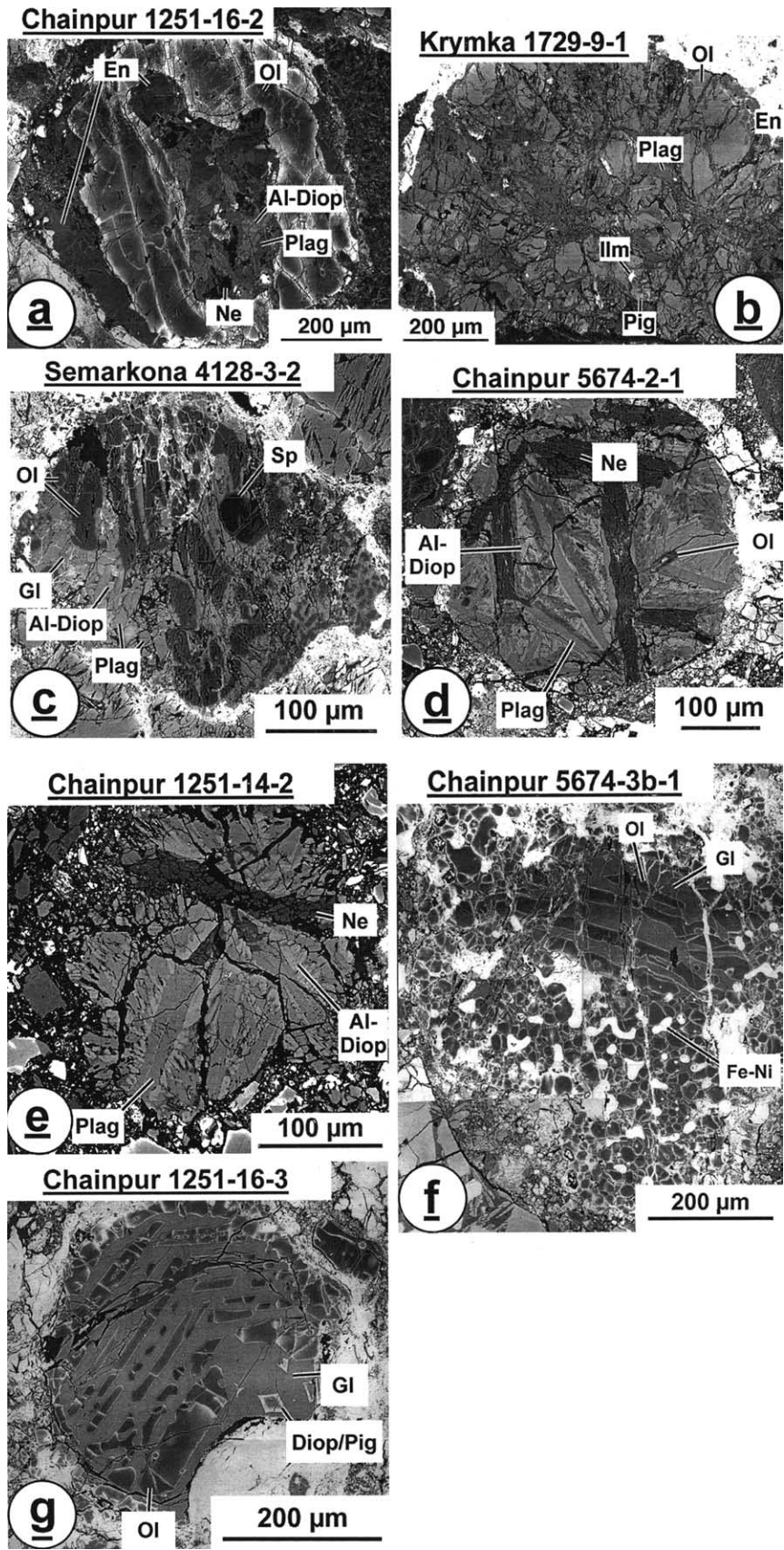
Nine of the eleven Al-rich chondrules in our study have textures dominated by olivine, either as large euhedral crystals or bars. Some of these also have spinel phenocrysts, but the spinel is subordinate to the olivine. Thus these nine chondrules can be described as olivine-phyric (porphyritic). Three of the olivine-phyric Al-rich chondrules are visually distinctive because they also contain abundant glass; in fact, their bulk chemistry (see below) is very different from that of the other olivine-phyric chondrules, and thus we can consider these glass-rich chondrules as a separate group. Textures of the two remaining chondrules are dominated by large euhedral plagioclase

laths, and therefore can be described as plagioclase-phyric. In all of the plagioclase-bearing chondrules, the feldspar is highly calcic in composition (mostly An >80, only rarely as low as An₆₆) and generally subhedral to euhedral in shape (i.e., other primary phases are to some degree subordinate to plagioclase in their shapes); for these reasons we consider it to be primary igneous plagioclase.

Bulk major and trace element compositions for the Al-rich chondrules are given in Table 7. The group has a very wide range of bulk chemical properties: e.g., Al₂O₃ ~3–28 wt.%, CaO <1–20 wt.%, MgO 5–40 wt.%. The two plagioclase-phyric chondrules, Chainpur 1251-14-2 and Chainpur 5674-2-1, have the greatest enrichments in calcium and aluminum of the entire group. The glass-rich chondrules (Chainpur 1251-16-3; Chainpur 5674-3b-1; Chainpur 1251-3-1) are characterized by high sodium contents, >2 to >8 wt.% Na₂O, low calcium contents in general (Chainpur 1251-16-3 and 5674-3b-1 contain only ~0.2 wt.% CaO), and the lowest calcium/aluminum ratios of the group. The remaining six, olivine-phyric, chondrules span a wide range of compositions but fall naturally into two groups, those with low (\leq 2 wt.%) FeO and those with \geq 5 wt.% FeO.

3.2. Comments on Nomenclature for Al-Rich Chondrules

The objects we studied were originally selected because they contain primary (igneous) aluminum-rich phases suitable for isotopic study. The bulk chemical compositions in Table 7 show, however, that four of these objects are not aluminum-rich chondrules as defined by Bischoff and Keil (1984), because they contain less than 10 wt.% Al₂O₃. We assert that this arbitrary cutoff is less important than the observation, elaborated below, that there exists a single family of objects having a continuum of compositions extending from type IA ferromagnesian chondrules at one extreme to the most plagioclase-rich CAIs at the other. It is the entire family of objects that we are concerned with here, and that family extends below the 10 wt.% Al₂O₃ limit used by Bischoff and Keil (1984). We do not wish at this time to propose a formal change to the definition (e.g., 5 or even 3 wt.% Al₂O₃); instead, we simply concede that



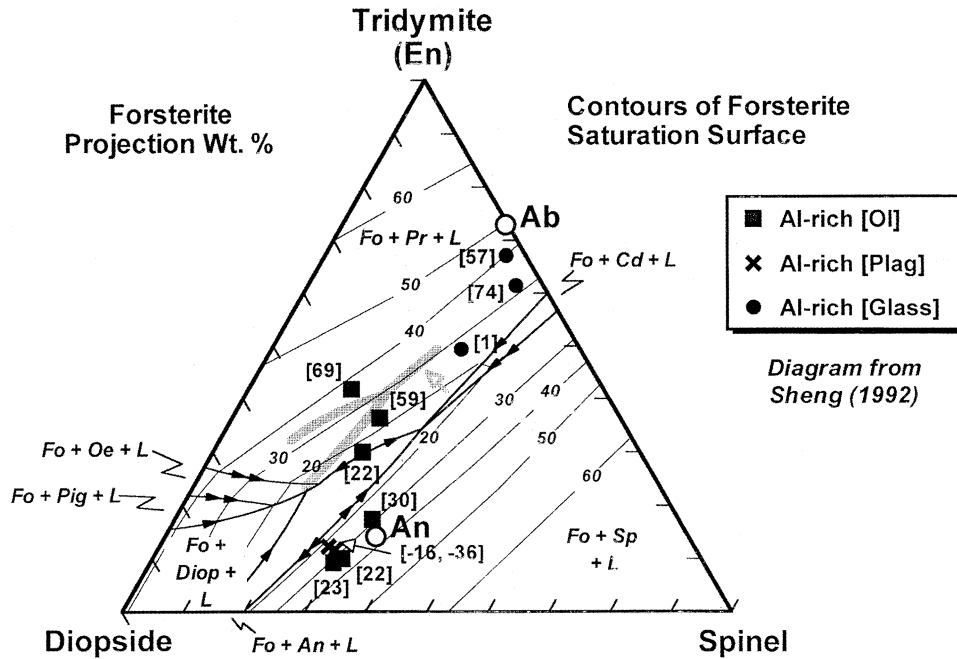


Fig. 2. Bulk compositions of all eleven Al-rich chondrules studied in this work, projected from forsterite onto the plane tridymite-diopside-spinel (Sheng, 1992). The composition of enstatite plots at the tridymite apex. Contours show the forsterite saturation surface, which defines the compositions of liquids coexisting with forsterite and one or more additional solid phases, and the numbers in brackets show the forsterite coordinate for each chondrule. On this and all subsequent phase diagrams, arrows on phase boundaries point down-temperature and double arrows mark reaction curves. Shaded boundaries show the effect of adding ~6 wt.% FeO to the bulk composition. Chondrules can be identified by their forsterite coordinates: Chainpur 1251-16-3 [57]; Chainpur 5674-3b-1 [74]; Chainpur 1251-3-1 [13]; Chainpur 1251-16-2 [69]; Krymka 1729-9-1 [59]; Quinyambie 6076-5-2 [22, on the An-Pr divide]; Semarkona 4128-3-2 [30]; Chainpur 1251-14-1 [22, in the Sp field]; Inman 5652-1-1 [23]; Chainpur 5674-2-1 [-16]; Chainpur 1251-14-2 [-36]. Abbreviations: Ab = albite; An = anorthite; En = enstatite; Fo = forsterite; Pr = protoenstatite; Cd = cordierite; Oe = orthoenstatite; Pig = pigeonite; Diop = diopside; Sp = spinel.

some of our objects do not fit that definition. However, we also are going to take some license and ignore it. We will continue to loosely apply the term “Al-rich chondrules” to this entire family of objects, even those with <10 wt.% Al₂O₃, because this will better allow us to explore the petrogenesis of the family of objects.

Bischoff and Keil (1984) correctly recognized that there are subtypes of Al-rich chondrules, but distinctions were

based on arbitrary chemical parameters (e.g., Na-Al-rich, Ca-Al-rich, Cr-Al-rich) etc. We follow a different approach, based on the relationship summarized above between major element chemistry and petrographic properties. We recognize two dominant varieties of Al-rich chondrules: those whose textures are dominated by early crystallizing olivine (± spinel), and those dominated by early crystallizing plagioclase (± spinel). These basic varieties arise from funda-

Fig. 1. Backscattered-electron images of seven Al-rich chondrules. (a) Chainpur 1251-16-2 is a complex Al-rich [Oliv] chondrule consisting of a core of enstatite (En), olivine (Ol), plagioclase (Plag), and aluminous diopside (Al-Diop) surrounded by a large optically continuous olivine crystal, which is in turn surrounded by a layer of enstatite and iron-rich olivine. Nepheline (Ne) partially replaces the plagioclase. (b) Krymka 1729-9-1 is an Al-rich [Oliv] chondrule fragment (~half) containing blocky olivine grains and interstitial plagioclase, exsolved pigeonite (Pig), and ilmenite (Ilm). Enstatite forms rims around the olivine at the periphery of the chondrule. (c) Semarkona 4128-3-2 is an Al-rich [Oliv] chondrule consisting of an incomplete set of olivine bars plus a large spinel (Sp) phenocryst with interstitial plagioclase, aluminous diopside, and silica-rich glass (Gl). Bright veins are the result of secondary alteration. (d) Chainpur 5674-2-1 is an Al-rich [Plag] chondrule consisting of large euhedral anorthitic plagioclase laths and a few blocky olivine grains set in a groundmass of aluminous diopside and a fine intergrowth of olivine, aluminous diopside, and plagioclase. Several plagioclase laths have been mostly replaced by nepheline. (e) Chainpur 1251-14-2 is an Al-rich [Plag] chondrule consisting of laths of anorthitic plagioclase with an interstitial intergrowth of anorthite and aluminous diopside. Some of the plagioclase has been replaced by nepheline. (f) Chainpur 5674-3b-1 is complex, and possibly compound, Al-rich [Glass] chondrule. The portion at upper right consisting of bars of olivine set in a groundmass of sodium-rich glass. The barred region is enclosed in a porphyritic assemblage of olivine, sulfide, and metal set in glass. (g) Chainpur 1251-16-3 is a beautiful example of an Al-rich [Glass] chondrule consisting of bars of olivine and a few small grains of pyroxene (pigeonite rimmed by diopside) in a groundmass of sodium-rich glass. A large metal-troilite nodule indents the chondrule at lower right.

Table 7. Bulk compositions of Al-rich chondrules (major and minor elements in wt. %, trace elements in ppm).

Sample	Chainpur 1251-16-2	Krymka 1729-9-1	Quinyambie 6076-5-2	Chainpur 1251-14-1	Inman 5652-1-1 ¹	Semarkona 4128-3-2	Chainpur 5674-2-1	Chainpur 1251-14-2	Chainpur 5674-3b-1	Chainpur 1251-16-3	Chainpur 1251-3-1
SiO ₂	45.99	42.83	46.58	40.32	41.87	43.45	44.72	44.14	33.50	34.80	51.66
TiO ₂	0.19	0.063	0.18	0.69	0.65	0.33	1.17	1.52	0.20	0.31	1.05
Al ₂ O ₃	3.49	6.17	12.30	16.39	16.21	15.92	22.57	27.79	4.43	5.90	19.42
Cr ₂ O ₃	0.41	0.25	ND	0.19	ND	0.29	0.22	0.022	0.076	0.19	0.14
FeO	5.82	12.34	9.21	0.69	1.90	0.39	0.90	0.20	1.63	2.03	0.99
MnO	0.14	0.064	ND	0.031	ND	0.16	0.020	0.012	0.021	0.033	0.025
V ₂ O ₃	0.018	0.008	0.015	0.043	0.014	0.039	0.011	0.010	0.005	0.002	0.014
NiO	0.011	0.041	ND	0.045	ND	0.010	0.006	0.032	0.020	0.014	0.027
MgO	40.41	34.84	21.71	26.61	27.80	29.51	12.39	5.39	31.28	23.49	11.08
CaO	3.06	3.61	8.18	11.17	11.80	8.87	17.55	20.35	0.21	0.23	4.51
Na ₂ O	0.21	0.25	1.26	0.44	0.026	0.25	0.29	0.46	2.46	3.45	8.26
K ₂ O	0.007	0.004	0.079	0.015	0.002	0.022	0.008	0.021	0.24	0.49	1.04
Fe ^o	0.53	0.069	0	2.70	0	0.58	0	0	19.48	17.76	1.29
Ni ^o	0.12	0.004	0	0.076	0	0.042	0	0	2.32	7.85	0.047
Co ^o	0.004	ND	0	0.011	0	0.002	0	0	0.15	0.099	0.013
Cr ^o	0.001	ND	0	ND	0	0.006	0	0	ND	0.031	0.001
S ^o	0.10	0	0	0.29	0	0.011	0	0	3.60	2.76	0.15
Total	100.51	100.54	99.51	99.71	100.27	99.88	99.86	99.95	99.62	99.44	99.72
Li	ND	3.1	1.1	0.058	0.31	ND	0.17	0.25	ND	ND	0.14
Be	ND	0.075	0.065	0.096	0.06	ND	0.29	0.42	ND	ND	0.45
Sc	26	23	31	44	77	35	94	82	20	25	81
Rb	6.1	7.7	6.0	0.60	1.39	1.5	0.78	1.66	8.3	13	33
Sr	47	39	103	111	38	47	177	319	1.5	0.57	3.9
Y	1.8	2.8	3.5	6.8	16	4.7	23	20	3.6	4.2	22
Zr	1.5	2.2	6.7	18	57	16	63	63	10	12	59
Nb	0.15	0.062	0.12	0.62	1.4	1.2	4.4	2.0	0.38	0.98	10
Ba	2.7	3.2	13	8.9	8.4	6.1	15	33	3.9	2.5	8.7
La	0.14	0.14	0.18	0.74	1.3	0.64	2.9	3.6	0.57	0.66	3.3
Ce	0.39	0.37	0.36	1.8	1.7	1.8	7.8	8.3	1.5	1.7	8.7
Pr	0.051	0.061	0.057	0.31	0.67	0.29	1.3	1.3	0.25	0.29	1.3
Nd	0.24	0.32	0.35	1.6	4.0	1.2	6.1	6.2	1.1	1.2	5.9
Sm	0.10	0.16	0.12	0.57	1.6	0.35	2.2	1.8	0.31	0.41	2.0
Eu	0.038	0.29	0.35	0.26	0.49	0.28	0.69	0.42	0.007	0.007	0.024
Gd	0.23	0.31	0.26	0.99	2.5	0.80	3.6	2.9	0.61	0.73	3.4
Tb	0.035	0.058	0.067	0.17	0.43	0.17	0.61	0.55	0.096	0.12	0.59
Dy	0.24	0.45	0.49	1.08	2.4	0.68	3.5	2.8	0.58	0.71	3.4
Ho	0.054	0.10	0.14	0.24	0.45	0.17	0.75	0.78	0.13	0.14	0.82
Er	0.20	0.39	0.34	0.78	1.6	0.53	2.7	2.1	0.41	0.51	2.6
Tm	0.026	0.092	0.089	0.11	0.32	0.12	0.43	0.40	0.071	0.082	0.44
Yb	0.25	0.35	0.43	0.79	1.5	0.61	2.8	2.3	0.41	0.57	2.7
Lu	0.034	0.070	0.077	0.11	0.30	0.094	0.37	0.29	0.073	0.094	0.42
Th	0.001	ND	ND	ND	ND	0.096	ND	ND	0.071	0.11	ND
U	ND	ND	ND	ND	ND	0.034	ND	ND	0.014	0.023	ND

ND = Not Determined.

¹ Composition of barred region only.

mental phase equilibrium considerations, as will be shown in this paper. We therefore will use the names Al-rich [Oliv] for the olivine-phyric Al-rich chondrules and Al-rich [Plag] for the plagioclase-phyric ones, in reference to their earliest-crystallizing silicate phases. The third variety, comprising those olivine-phyric chondrules with abundant sodium-aluminum-rich glass, are separately termed Al-rich [Glass] chondrules. For comparison, most of the plagioclase-olivine inclusions of Sheng et al. (1991) (Ca-Al-rich chondrules in the terminology of Bischoff and Keil, 1984) are Al-rich [Plag] chondrules in our system; the rest are Al-rich [Oliv] chondrules that are rich in modal plagioclase. Note that the nomenclature system used herein for Al-rich chondrules differs slightly from that described in Huss et al. (2001).

3.2. Phase Equilibria and Crystallization Sequences in Al-Rich Chondrules

Treating Al-rich chondrules as true chondrules assumes that they crystallized entirely from homogeneous melts. However, Al-rich chondrule-like objects have been reported elsewhere in which the aluminous phases are plausibly xenocrysts and thus did not crystallize from a chondrule melt. For example, Sheng et al. (1991) used magnesium isotopic measurements to argue that spinel in some plagioclase-olivine inclusions is xenocrystic in origin. However, some chondrules clearly contain relict fragments of whole CAIs within them (e.g., Krot et al., 2002; Krot and Keil, 2002; Krot et al., 2004b). The existence of compound objects such as these naturally raises the question of whether any of the Al-rich objects in this study might also

contain xenolithic material, trapped in otherwise ordinary ferromagnesian chondrule melts. We can test this by determining if the observed mineral crystallization sequences in our chondrules are consistent with the predictions of relevant phase equilibria for their individual bulk composition. This test can in principle be accomplished in either of two ways: plotting bulk compositions on suitable phase equilibrium diagrams, or using a numerical liquid crystallization program (e.g., MELTS) to calculate the liquid line-of-descent for each individual composition.

Our approach herein relies primarily on experimentally determined phase equilibrium diagrams within the CaO-MgO-Al₂O₃-SiO₂ (CMAS) system. For our purposes, melt-crystallization programs such as MELTS (Ghiorso, 1985; Ghiorso and Sack, 1995) have only limited utility because they are designed primarily for terrestrial and planetary magmas that contain abundant iron, alkalis, and silica. Thus MELTS works well for basalt compositions, but it does not work well at all for calcium-aluminum-rich and iron-silicon-poor compositions like those of many of our chondrules. We can and do use MELTS calculations for additional insight into those iron-rich chondrules whose crystallization sequences cannot accurately be depicted on our diagrams.

To properly visualize the phase relations of Al-rich chondrules as a group it is necessary to consider more phases—plagioclase, olivine, low- and high-calcium pyroxene, and spinel—than can be portrayed in any single two-dimensional phase diagram. One partial solution to this problem is to use phase-projection diagrams that portray phase relationships in a system saturated with a common (liquidus) phase. This permits a four-component system to be depicted accurately within a two-dimensional diagram. We have already emphasized that most Al-rich chondrules have either olivine or plagioclase as their liquidus (saturated) phase, and Sheng (1992) took advantage of this fact to construct two very useful ternary phase projections for the purpose of studying the crystallization sequences of Al-rich chondrules. One diagram is relevant to olivine-saturated equilibria and the other to plagioclase-saturated equilibria. Both are constructed for melts whose compositions are described entirely by the CMAS system (in these and ensuing discussions of crystallization sequences, we ignore the effects of metal and sulfide). Setting aside for now the fact that some of our chondrules contain significant iron and sodium, Figure 2 shows the bulk compositions of all eleven Al-rich chondrules projected from forsterite onto the plane tridymite-diopside-spinel, along with contours on the olivine-saturation surface. The number in brackets next to each symbol is the forsterite coordinate for each chondrule. If the coordinate is greater than the value for the contour of the forsterite saturation surface at that point, forsterite is the liquidus phase for the equivalent melt of that composition. Otherwise, forsterite is not the liquidus phase. Of the six Al-rich [Oliv] chondrules, shown as filled squares in Figure 2, four (Semarkona 4128-3-2, Qinyambie 6076-5-2, Chainpur 1251-16-2, Krymka 1729-9-1) plot on or above the forsterite saturation surface. The other two (Inman 5652-1-1, Chainpur 1251-14-1) plot somewhat below the olivine saturation surface in the spinel field. Two of the three Al-rich [Glass] chondrules (Chainpur 1251-16-3; Chainpur 5674-3b-1; shown as filled circles in Fig. 2) plot above the forsterite saturation surface at the calcium-poor edge of the

protoenstatite field, consistent with their having olivine phenocrysts. The third Al-rich [Glass] chondrule, Chainpur 1251-3-1 (also a filled circle) plots far below the forsterite saturation surface. The two Al-rich [Plag] chondrules (Chainpur 1251-14-2, Chainpur 5674-2-1; shown as crosses in Fig. 2) plot so far below the forsterite saturation surface that Figure 2 is not useful for evaluating their crystallization histories. Their compositions are plotted separately on Figure 3, which is the same plane (tridymite-diopside-spinel) but projected from anorthite instead of forsterite; both plot well above the plagioclase saturation surface.

In detail, only five of our Al-rich chondrules have sufficiently low FeO and Na₂O contents that the phase relationships as shown on Figures 2 and 3 are applicable throughout the liquid lines of descent. Three are Al-rich [Oliv] chondrules and plot just within the spinel field in Figure 2; Chainpur 1251-14-1 and Inman 5652-2-1 lie slightly below the forsterite saturation surface, and Semarkona 4128-3-2 lies above it. Because Chainpur 1251-14-1 (Fo coordinate of [22] on Fig. 2) plots within the spinel field just below the forsterite saturation surface on Figure 2, spinel likely will crystallize first, moving the composition away from spinel until it intersects the forsterite saturation surface, where forsterite begins to crystallize. The path of the residual melt continues on to intersect the spinel-anorthite (+ forsterite) reaction curve, where plagioclase begins to crystallize and spinel begins to react with the liquid. Once spinel disappears, diopside begins to crystallize and the liquid composition evolves across the plagioclase field to encounter the pyroxene boundary. This is in reasonable agreement with the olivine and spinel phenocrysts (spinel enclosed in olivine) and plagioclase and pyroxene groundmass in this chondrule. For Inman 5652-1-1, the interior barred region (on which the mode in Table 1 is based) plots close to Chainpur 1251-14-1 (Fig. 2) and the predicted crystallization sequence is the same: spinel, followed by forsterite, then plagioclase, and finally pyroxene, consistent with the sequence inferred from petrography. Semarkona 4128-3-2 illustrates the effect even a small amount of sodium has on the phase relationships. This chondrule seemingly has the wrong pyroxene: Its bulk composition lies on the opposite side of a thermal divide along the plagioclase-spinel cotectic in Figure 2 from the other two chondrules, so that once olivine, spinel, and plagioclase appear in that order, the melt should evolve toward the protoenstatite field. The position of the thermal divide is defined by a line drawn between anorthite and spinel, extended to the cotectic. However, the plagioclase in Semarkona 4128-3-2 is ~An₈₃, which plots somewhat up and to the right of anorthite in the direction of albite (Ab, on the tridymite-spinel side of the ternary). The position of the thermal divide appropriate to this chondrule is thus up the anorthite-spinel cotectic sufficiently far that the bulk composition of the Semarkona chondrule does evolve into the diopside field. Thus, the three iron-poor Al-rich [Oliv] chondrules have mineral assemblages consistent with the predictions of phase-equilibrium constraints.

The Al-rich [Plag] chondrules (Chainpur 5674-2-1 and 1251-14-2) plot above the anorthite saturation surface on Figure 3, consistent with textural evidence that plagioclase was the earliest phase to begin crystallizing. Chainpur 1251-14-2 plots far above the anorthite saturation surface, just within the forsterite field and close to the diopside/forsterite boundary curve. The

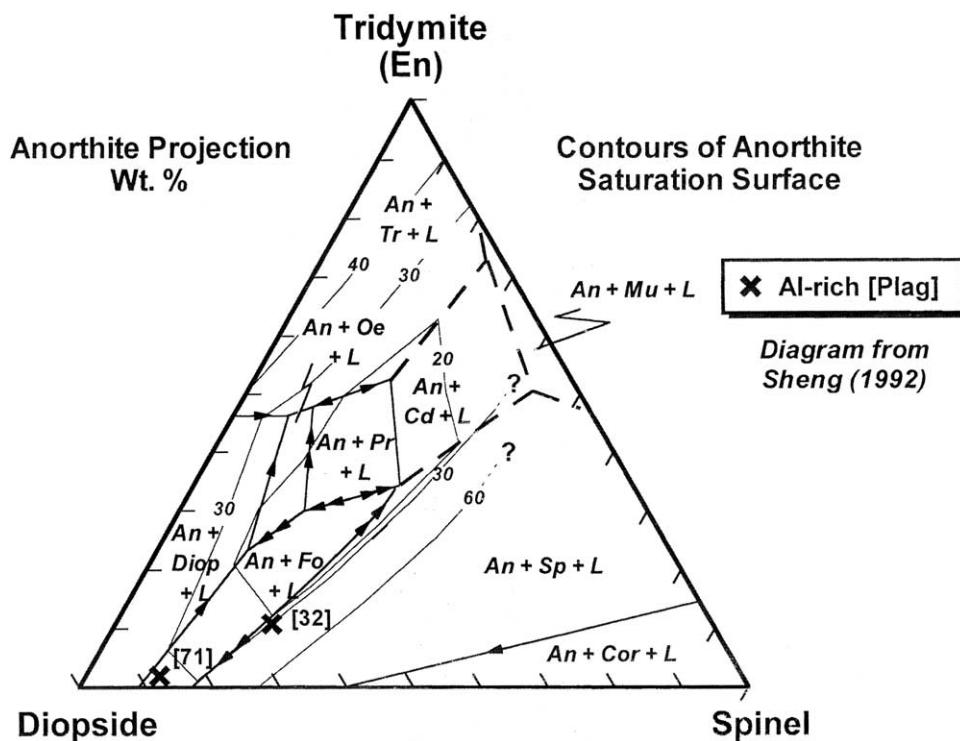


Fig. 3. Bulk compositions of the two Al-rich [Plag] chondrules, Chainpur 5674-2-1 and Chainpur 1251-14-2, projected from anorthite onto the plane tridymite-diopside-spinel (Sheng, 1992). All of the other nine chondrules would plot far below the plagioclase saturation surface and thus it is not appropriate to plot them on this diagram. Contours show the anorthite saturation surface and the numbers in brackets show the anorthite coordinate for each chondrule. Chondrules can be identified by their anorthite coordinates: Chainpur 5674-2-1 [32]; Chainpur 1251-14-2 [71]. Abbreviations: Cor = corundum; Mu = mullite; others as in Figure 2.

predicted crystallization sequence is anorthite, followed by forsterite, then diopside; this sequence does not change, even accounting for the small amount of sodium in the actual feldspar. In fact, diopside fills in between the anorthite laths and there is no forsterite anywhere. A small error in the mode might account for the discrepancy, given that the bulk composition plots so close to the diopside field. However, the dendritic interstitial textures and unusual Al-rich pyroxene chemistry hint at very rapid crystallization, rendering the phase relationships on Figure 3 less accurate and possibly resulting in enhanced stability field for the pyroxene. Chainpur 5674-2-1 plots just to the spinel side of the forsterite/spinel boundary, effectively on the anorthite saturation surface. The expected crystallization sequence will be anorthite plus a small amount of spinel first (order unclear), then forsterite, and finally diopside. The complete absence of spinel from Chainpur 5674-2-1 can reasonably be expected from the fact that any early-formed spinel will be in reaction relationship with the liquid along the forsterite/spinel boundary curve, once olivine begins to cocrystallize with plagioclase. The only requirement is that the small amount of spinel not become trapped in another phase and thereby isolated from reaction with the liquid.

The three Chainpur Al-rich [Glass] chondrules (5674-3b-1, 1251-16-3, 1251-3-1) contain several weight percent Na_2O and, although the bulk compositions are not notably FeO-rich, the residual glasses in the chondrules have $(\text{Fe}/(\text{Fe}+\text{Mg})) \approx 0.6-0.7$. Therefore, predictions of crystallization sequences

based on Figure 2 are inaccurate much beyond the liquidus phase itself. To appreciate the problem, consider the following qualitative effects. Elevated sodium has the effect of expanding the olivine field at the expense of spinel, expanding the spinel field at the expense of cordierite, and suppressing plagioclase crystallization (Longhi and Pan, 1988; Sheng, 1992). During progressive crystallization the plagioclase field continues to shrink, and so too (with increasing Fe/Mg) do the fields of both protoenstatite and orthoenstatite relative to that of pigeonite (Longhi and Pan, 1988). Chainpur 5674-3b-1 and 1251-16-3 both plot near the spinel-tridymite join on Figure 2, within the low-Ca pyroxene field and well above the forsterite saturation surface. Thus the initial expected crystallization sequence for both is olivine, possibly followed by low-Ca pyroxene. MELTS predicts olivine, trace spinel (nominally an Mg-Al-rich chromite, due to the fact that MELTS forces all chromium into spinel instead of silicates), and sodic plagioclase for both, with no low calcium pyroxene. Chainpur 5674-3b-1 contains only olivine and glass (plus metal and troilite); Chainpur 1251-16-3 contains olivine, glass, and a trace amount of pyroxene (pigeonite mantled by diopside). Thus, assuming that the feldspar component is contained in the glass, the observed sequences are broadly consistent with predictions. The calculated bulk composition for Chainpur 1251-3-1 plots well below the forsterite saturation surface on Figure 2, within the low-calcium pyroxene field. The expectation therefore is that the early crystallizing phases will be low calcium pyroxene and olivine. This is at

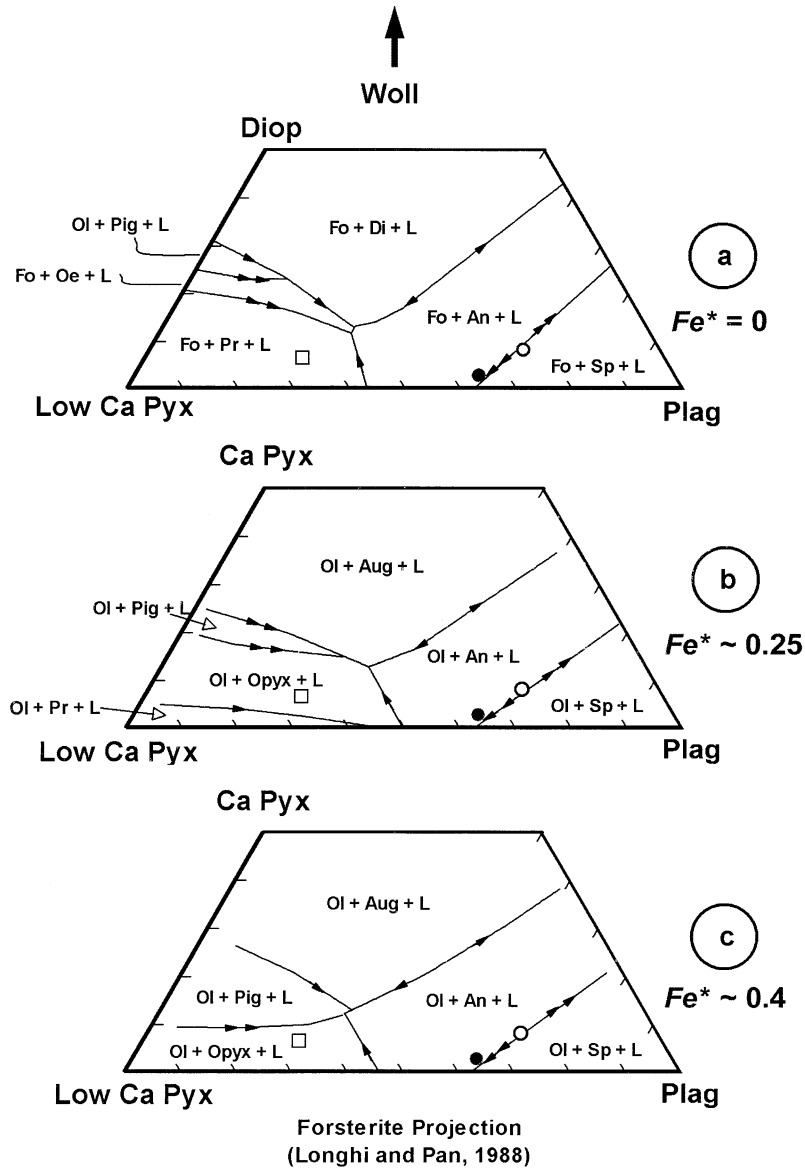


Fig. 4. Bulk compositions of Chainpur 1251-16-2 (open square), Krymka 1729-9-1 (filled circle), and Quinyambie 6076-5-2 (open circle) are projected from forsterite onto a portion of the plane wollastonite-low-Ca pyroxene-plagioclase. The diagram, in oxygen units, is from Longhi and Pan (1988). Phase boundary curves for the Fe-free system (molar $FeO/[FeO + MgO] \equiv Fe^* = 0$) are shown in panel a, and curves for two Fe-bearing compositions ($Fe^* = 0.25$, $Fe^* = 0.4$) are shown in panels b and c.

variance with the observed abundant olivine and spinel phenocrysts. The spinel crystals have rounded shapes and might plausibly be interpreted as xenocrysts. The sharply defined skeletal shapes of the olivine crystals might argue for rapid crystallization, but they are not xenocrysts. Here MELTS is more helpful: the calculated crystallization sequence is spinel (albeit still a trace, and chromium-rich) followed by olivine, low-calcium pyroxene, and diopside. The observed spinel crystals may indeed be xenocrysts, but the remaining sequence is consistent with the predictions of MELTS.

The remaining three Al-rich [Oliv] chondrules have elevated FeO contents, which significantly affect the phase relationships shown in Figure 2. Of particular significance to the crystalli-

zation sequences in these chondrules is that high FeO causes the fields of both protoenstatite and orthoenstatite to shrink relative to that of pigeonite. Because FeO will tend to increase in a residual liquid with progressive crystallization, these effects will increase accordingly. Fortunately, two supplemental tools enable us to describe more accurately the liquid lines of descent of these three chondrules. First, the effect of iron on the system wollastonite-enstatite-anorthite was examined in detail by Longhi and Pan (1988); one of their diagrams (Fig. 4) visually illustrates how the crystallization sequences of these chondrules change as a result of elevated FeO contents. Second, these three objects have compositions well suited to MELTS calculations of the crystallization sequences and com-

positions of the crystallizing phases as functions of falling temperature.

Looking first at [Figure 2](#), the chondrules Quinyambie 6076-5-2, Chainpur 1251-16-2, and Krymka 1729-9-1 contain significant modal low-Ca pyroxene and plot within the protoenstatite field above the forsterite saturation surface. For all three, therefore, in the Na-Fe-free system, the expected crystallization sequence is olivine followed by protoenstatite (olivine dissolving by reaction with the liquid), plagioclase, and either orthoenstatite followed by diopside (Quinyambie 6076-5-2, Chainpur 1251-16-2) or else cordierite (Krymka 1729-9-1), depending on which side of the thermal divide on the protoenstatite/anorthite boundary curve the evolving residual liquid reaches. [Figure 4](#) shows the same three chondrules projected from forsterite onto a portion of the plane wollastonite–low-Ca pyroxene–plagioclase, with phase boundary curves for the Fe-free system (molar $\text{FeO}/(\text{FeO} + \text{MgO}) \equiv Fe^* = 0$) and for two Fe-bearing compositions ($Fe^* = 0.25$, $Fe^* = 0.4$). The latter two diagrams illustrate the significant effect of elevated FeO (or increasing Fe^* in residual liquids) on the topology of the various pyroxene fields and the consequences for crystallization of the three chondrules. Chainpur 1251-16-2 has the lowest FeO of the three ($Fe^* \approx 0.05$) and plots in a low-Ca pyroxene field on all three diagrams. In the Fe-free system ([Fig. 4a](#)) the expected crystallization sequence is forsterite–(proto)enstatite–anorthite. But, because early crystallizing ferromagnesian phases are magnesium rich relative to the liquid, progressive crystallization will drive Fe^* up. At $Fe^* \approx 0.25$ (middle diagram) the sequence becomes olivine–low-Ca pyroxene–anorthite–augite, which is the observed assemblage in Chainpur 1251-16-2. MELTS basically predicts the same sequence as [Figure 4](#) except for the spurious appearance of a trace amount of chrome spinel after olivine, and a failure to predict the appearance of augite. Krymka 1729-9-1 has bulk $Fe^* \approx 0.17$, meaning that [Figure 4b](#) approximates the phase topology for the beginning of its crystallization. The expected crystallization sequence is olivine–anorthite–low-Ca pyroxene–augite. By the time crystallization of early Mg-rich silicates has driven Fe enrichment to $Fe^* \approx 0.4$, the pigeonite field has greatly expanded at the expense of low-Ca pyroxene, and pigeonite is expected as the final crystallizing phase of Krymka 1729-9-1, consistent with observation. The expectation from [Figure 2](#) that cordierite might be a late stage phase in Krymka 1729-9-1 cannot be evaluated from [Figure 4](#), because [Longhi and Pan \(1988\)](#) did not study bulk compositions as Al rich as those in [Sheng's \(1992\)](#) work. It is not, in any case, actually present in the chondrule, and we can only surmise that the elevated Fe content of the evolving melt destabilized cordierite relative to pyroxene ([Sheng, 1992](#)). MELTS predicts the crystallization sequence of Krymka 1729-9-1 to be olivine, trace spinel (spurious chromite again), plagioclase, low-Ca pyroxene, and aluminous augite. This is approximately consistent with petrography except for the actual presence of pigeonite instead of augite. Finally Quinyambie 6076-5-2 ($Fe^* \approx 0.19$) should behave in a manner similar to the Krymka chondrule, except that augite will be the first pyroxene and there is no expectation (based on [Fig. 2](#)) of cordierite under any circumstances. MELTS predicts the

following sequence for this object: olivine, plagioclase, sub-calcic augite, and low-Ca pyroxene.

In summary, the observed crystallization sequences in most of the Al-rich chondrules we studied are in reasonable agreement with the predicted phase equilibria for the respective bulk compositions. Only in chondrule Chainpur 1251-3-1 can the large and unexpected spinel crystals plausibly be interpreted as xenocrysts. All the others appear to have crystallized entirely from melts and are true chondrules.

3.3. Elemental Abundance Patterns of Al-Rich Chondrules

Elemental abundance patterns are useful to investigate the chemical characteristics of the chondrule precursors and the chemical fractionations produced during chondrule formation. The abundances of nearly 40 elements are plotted for each chondrule relative to CI abundances in [Figures 5–7](#). In these figures, the elements are arranged from left to right in order of decreasing volatility. Because the data have not been normalized to any individual element, depletions in some elements relative to CI composition result in enrichments in the remaining elements.

[Figure 5](#) shows the abundance patterns for the six Al-rich [Oliv] chondrules. The three chondrules with significant bulk FeO (Chainpur 1251-16-2, Krymka 1729-9-1, Quinyambie 6076-5-2) have overall abundances for most elements within a factor of three of CI abundances, independent of volatility. The rare-earth elements (REE) are slightly fractionated with light rare earths (LREE) depleted by factors of 1.5 to 3 relative to heavy rare earths (HREE). There are several clear exceptions to these general rules. The most volatile elements (sulfur, sodium, and potassium) are depleted in two of the chondrules. The siderophile elements (iron, nickel, and cobalt) are depleted in all three chondrules, consistent with loss of metal as an immiscible metal melt during chondrule formation ([Grossman et al., 1988](#); [Connolly et al., 2001](#)). Zirconium is markedly depleted relative to aluminum and scandium in all three chondrules, and uranium and thorium are severely depleted in Chainpur 1251-16-2. In all three chondrules, strontium, calcium, and aluminum show correlated enrichments relative to refractory elements (e.g., the REE), and all three have small (Chainpur 1251-16-2) or large (Krymka 1729-9-1, Quinyambie 6076-5-2) positive europium anomalies. These correlated enrichments suggest enrichment of plagioclase in the chondrule precursor.

Relative to the chondrules just discussed, the remaining three, FeO-poor, Al-rich [Oliv] chondrules (Semarkona 4128-3-2, Chainpur 1251-14-1, Inman 5652-1-1) have higher overall abundances of all elements more refractory than beryllium ($3\text{--}5 \times \text{CI}$ in Semarkona 4128-3-2 and Chainpur 1251-14-1, and $\sim 10 \times \text{CI}$ in Inman 5652-1-1) ([Fig. 5](#)). All three chondrules show relative depletions in the more volatile elements, with the most volatile being most strongly depleted. All three chondrules are also depleted in siderophile elements, consistent with low metal abundances. Depletions of volatile and siderophile elements are responsible for the increased abundances of refractory lithophile elements (cf. [Fig. 7](#)). Semarkona 4128-3-2 and Chainpur

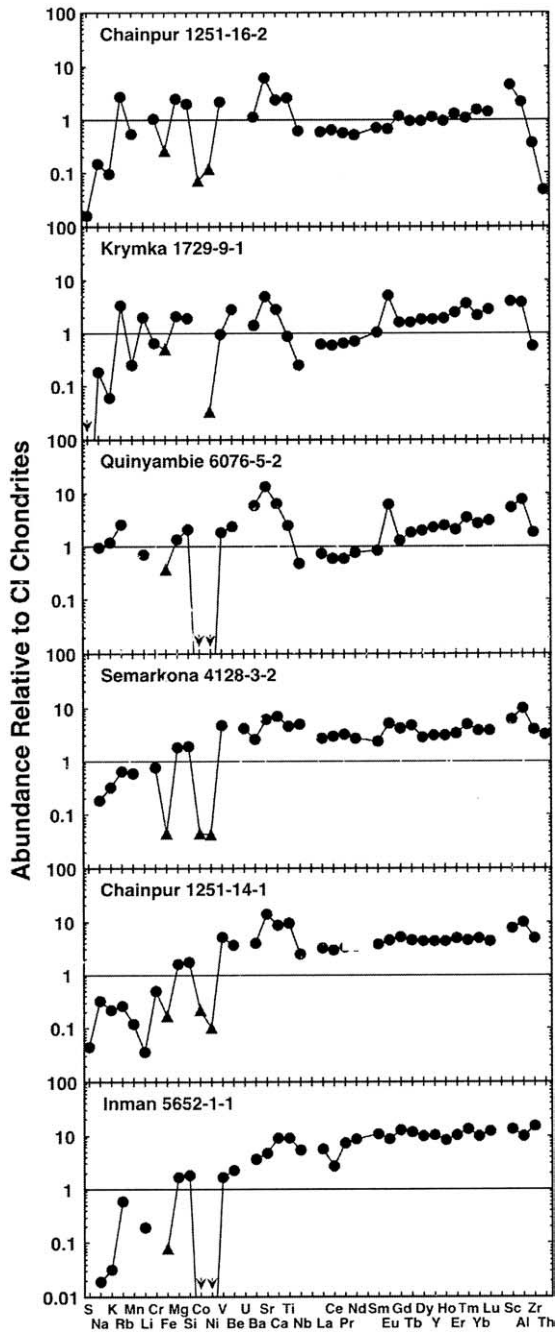


Fig. 5. Elemental abundances in Al-rich [Oliv] chondrules, normalized to CI chondrites (from Anders and Grevesse, 1989). Elements here and in Figures 6 and 7 are arranged in order of decreasing volatility in a gas of solar composition, except for the rare earths, which are in order of atomic number. Abundances for most elements in the high-FeO chondrules (Chainpur 1251-16-2, Krymka 1729-9-1, Quinyambie 6076-5-2) are close to solar, and the REE show slightly fractionated patterns with heavier REE enriched over lighter REE. Iron, Ni, and Co (all highlighted as triangles) are depleted compared to adjacent elements, suggesting loss of metal from the chondrules. Calcium, Sr, Eu (in two of three cases), and Al, which have a wide range of volatility, are similarly enriched relative to CI abundances, suggesting addition of plagioclase to the chondrule precursor. Abundances for most elements in the low-FeO chondrules (Semarkona 4128-3-2, Chainpur 1251-14-1, Inman 5652-1-1) are enriched relative to solar, and the REE patterns are essentially unfractonated. Iron, Ni, and Co again show correlated depletions relative to adjacent elements, suggesting metal loss.

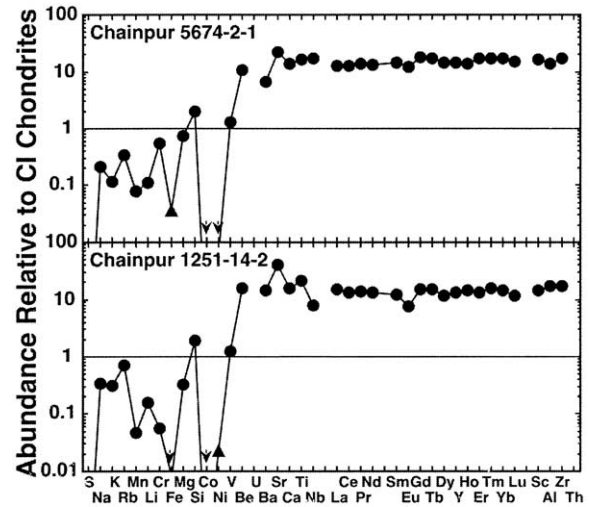


Fig. 6. Elemental abundances in Al-rich [Plag] chondrules, normalized to CI chondrites. Refractory elements are significantly enriched relative to CI abundances, with the degree of enrichment increasing from top to bottom in the figure. Both chondrules have high normative anorthite contents yet have negative Eu anomalies. Note the correlated depletions of Fe, Ni, and Co (all highlighted as triangles), which suggest loss of metal from the chondrules.

1251-14-1 show enrichments of strontium, calcium, and aluminum relative to surrounding elements, and Semarkona 4128-3-2 has a hint of a positive europium anomaly. These enrichments could point to addition of plagioclase to the precursor, but the enrichments are small enough that they may simply reflect incorrect modal abundances for the chondrules due to unrepresentative sampling of the minerals in the section that we studied. Inman 5652-1-1 shows a moderate negative anomaly in cerium and the entire REE pattern shows increasing depletion with increasing volatility for elements more volatile than gadolinium (Fig. 5). This trace element pattern suggest that a volatility-related process (condensation, evaporation) played a role in the formation of Inman 5652-1-1. Cerium is volatile under oxidizing conditions, as shown by evaporation experiments on a variety of starting materials (e.g., Davis et al., 1995; Floss et al., 1996). In these experiments, evaporation of major-element oxides released large amounts of oxygen that locally increased the oxygen fugacity and permitted cerium (and vanadium) to evaporate as oxides.

The two Al-rich [Plag] chondrules (Fig. 6), Chainpur 1251-14-2 and Chainpur 5674-2-1, have large roughly constant enrichments relative to CI of all elements more refractory than Be ($10\text{--}20 \times$ CI in both chondrules). Both chondrules show major depletions in siderophile elements, consistent with the absence of metal. Volatile elements show generally increasing depletions with increasing volatility, although Chainpur 1251-14-2 is not as depleted in alkalis as expected from the trend of other volatile elements. The REE patterns are flat except for small negative Eu anomalies.

The three Al-rich [Glass] chondrules are characterized by large negative europium anomalies superimposed on flat REE patterns enriched to $3\text{--}10 \times$ CI (Fig. 7), depletions in calcium and strontium relative to the more refractory ele-

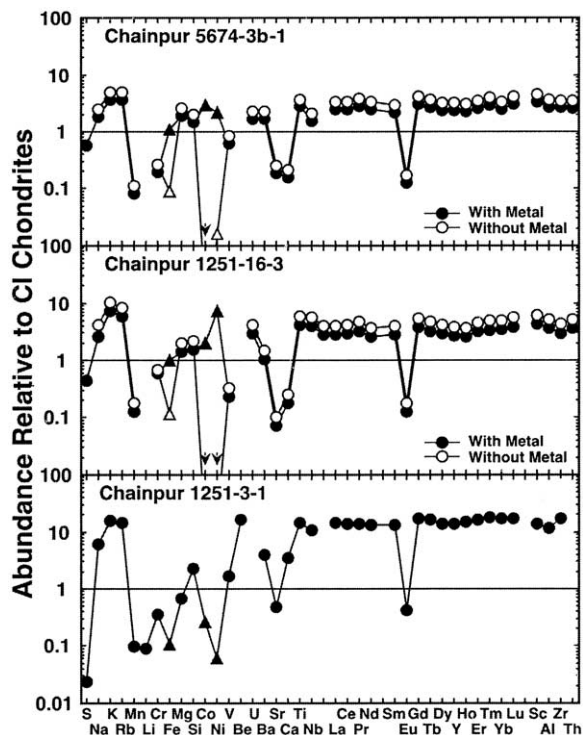


Fig. 7. Elemental abundances in Al-rich [Glass] chondrites. Refractory elements are enriched relative to CI abundances and have a flat pattern except for correlated depletions in Eu, Sr, and Ca. Correlated depletions of Fe, Ni, and Co (again highlighted as triangles) in Chainpur 1251-3-1 suggest metal loss. Chainpur 1251-16-2 and Chainpur 5674-3b-1 contain large amounts of metal and have essentially undepleted siderophiles. The open symbols for these two chondrites show the effect of metal loss on the abundance patterns.

ments, and enrichments in sodium and potassium to about the same level as the refractory elements. These features are unique to the Al-rich [Glass] chondrites. The enrichments of refractory elements and the depletions of moderately volatile elements and europium are consistent with volatility control, but the high sodium and potassium abundances and large depletions in calcium and strontium imply a more complicated history than experienced by the other Al-rich chondrites. Iron and siderophile elements are depleted in Chainpur 1251-3-1, but are not unusually low in the other two chondrites, both of which contain large amounts of metal. During the chondrule melting event(s), siderophile elements commonly form an immiscible metal melt that can be ejected from the chondrule (e.g., Grossman et al., 1988). Most of the metal in Chainpur 1251-16-3 consists of a single large metal-sulfide grain located at the surface of the chondrule which looks as if it were about to be expelled (Fig. 1d). If the metal grain is excluded from the calculation of the bulk composition, as it would have been if the molten metal droplet had been lost from the chondrule, depletions of siderophile elements like those in Chainpur 1251-14-1, 5674-2-1, 1251-14-2, and 1251-3-1 and Inman 5652-1-1 are observed (Fig. 7; cf. Figs. 5 and 6). The exclusion of metal also results in increased abundances of the lithophile elements in the chondrule. A similar calculation was also done for Chainpur 5674-3b-1 (Fig. 7).

4. DISCUSSION

4.1. Al-Rich Chondrules, CAIs, and Ferromagnesian Chondrules: Relationships and Petrogenetic Insights Based on a Cosmochemical Phase Diagram

Al-rich chondrules have long been recognized as a special group of objects that share some properties both with “normal” ferromagnesian chondrules and with CAIs and yet are distinct from both (e.g., Nagahara and Kushiro, 1982; Bischoff and Keil, 1984; Bischoff et al., 1989; McCoy et al., 1991; Sheng et al., 1991). Most previous workers have looked at either a very limited number of objects or else those of a particular restricted type, and what has been lost as a result is a sense of the great variety of Al-rich chondrules and the causes of that variety. The first attempt at a systematic study of these objects was by Bischoff and Keil (1984), who recognized their diverse, yet continuous, chemistry and mineralogy. Wark (1987) recognized that some Al-rich chondrules merge in their properties with the variety of CAI known as type C. Sheng et al. (1991) and Sheng (1992) studied a group of objects that they named plagioclase-olivine inclusions (POIs) and which are, in fact, mostly Al-rich [Plag] chondrules. What has been lacking is any petrogenetic understanding of how and why the varieties of Al-rich chondrules are related to one another or how they relate to CAIs and ferromagnesian chondrules.

Relating the bulk chemistry of CAIs, Al-rich chondrules, and ferromagnesian chondrules in graphical form has proven difficult or ineffective in the past. Conventional phase diagrams are too limited in compositional range to represent more than a subset of this combined group of objects. Simple ternary oxide diagrams cannot represent more than three of the essential CMAS components without combining two of them (e.g., Huang et al., 1996), which results in loss of significant information. We therefore again have adopted a projection method, in this case based on that of Stolper (1982), which takes advantage of the fact that most CAIs and many (not all) Al-rich chondrules have spinel ($MgAl_2O_4$) as an early-crystallizing phase. By projecting from spinel and showing only spinel-saturated phase equilibria, the number of phases to be portrayed graphically is reduced by one. Unlike the ternary system chosen by Stolper (1982), however, we project onto the plane Ca_2SiO_4 – Mg_2SiO_4 (Fo: forsterite)– Al_2O_3 (Cor: corundum) because it allows a much greater range of solar-system materials than just CAIs to be plotted in a single diagram. The diagram is constructed using experimental phase equilibrium data taken from the literature. Figure 8 illustrates the projection scheme (Fig. 8a), the phase relationships with isotherms (Fig. 8b), and the phase relationships with contours of the spinel saturation surface (Fig. 8c). One aspect of the diagram requires careful explanation. Both the spinel saturation surface and the compositions of many chondrules and CAIs plot well below the projection plane itself, with the result that the spinel coordinates (the distance above or below the plane of the graph) generally have large negative values. While perhaps unsettling, this circumstance is unimportant; the phase relationships are completely valid, and what matters is the value of the spinel coordinate of a particular CAI or chondrule bulk composition *relative* to that of the spinel saturation surface

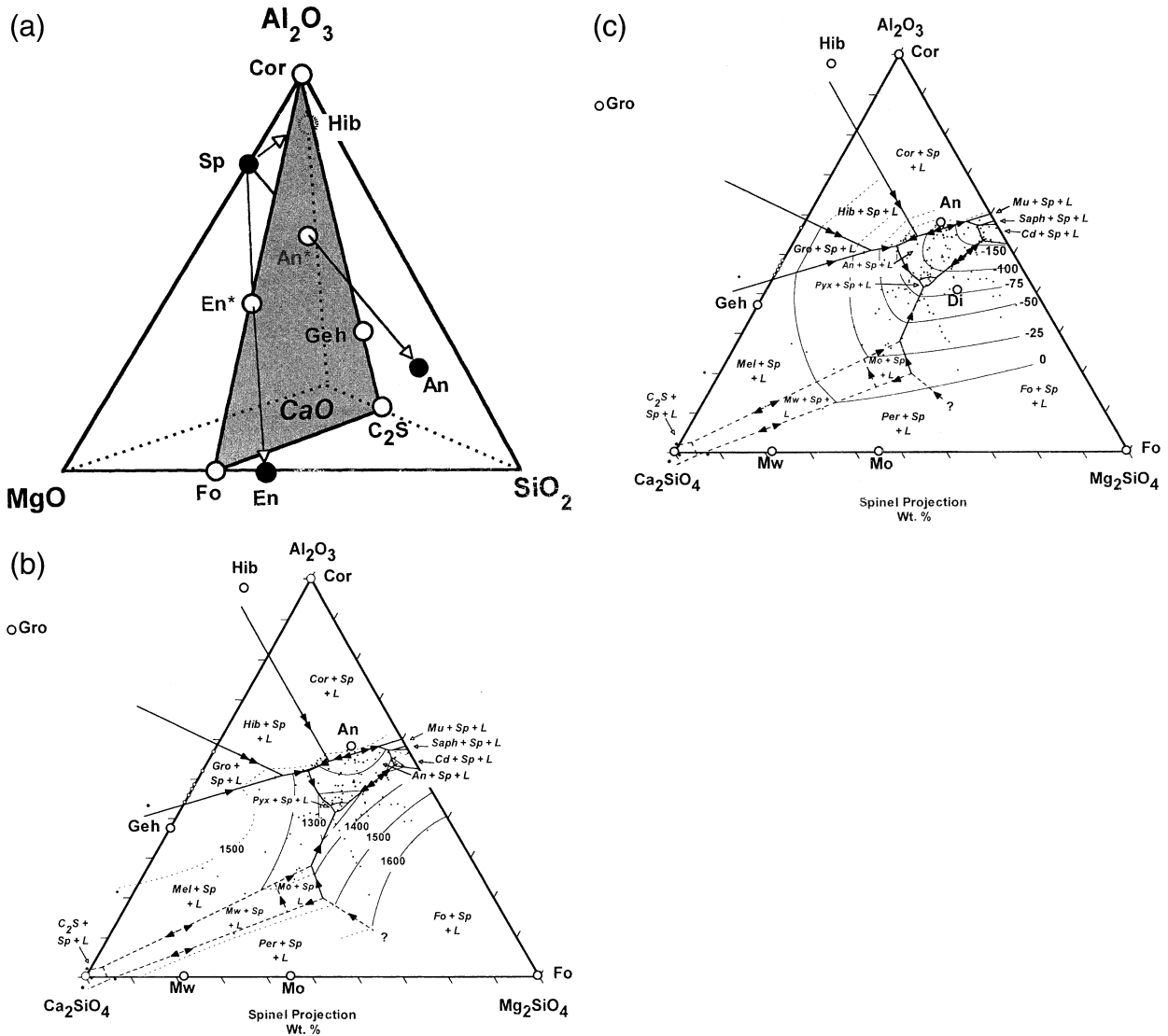


Fig. 8. A cosmochemical phase diagram. (a) The projection scheme within the CaO-MgO-Al₂O₃-SiO₂ system, from MgAl₂O₄ (spinel) onto the plane Ca₂SiO₄ (C₂S)-Mg₂SiO₄ (Fo)-Al₂O₃ (Cor). (b) The spinel-saturated liquidus relationships on the phase diagram, together with isotherms contours. Points show the experimental data (taken from literature) from which the diagram was constructed. (c) The contours of the spinel saturation surface. In this projection the saturation surface has the form of a trough that dips steeply down below the plane of the diagram (large negative spinel coordinates) in the direction of cordierite-sapphirine-mullite. Note that the ternary projection used by Stolper (1982) to represent CAIs, gehlenite-forsterite-anorthite, is contained within this system, but only its base (gehlenite-forsterite) actually lies in the plane of this diagram and the plane itself dips steeply downward toward anorthite. Experimental data taken from references compiled in Stolper (1982), Sheng (1992), and Beckett and Stolper (1994), plus additional data from Prince (1951), Osborne et al. (1969), and Rao (1968). Abbreviations: An = anorthite, Cor = corundum; Cd = cordierite, Fo = forsterite, Geh = gehlenite, Gro = grossite; Hib = hibonite; Mu = mullite, Mel = melilite solid solution; Mw = merwinite; Mo = monticellite; Per = periclase, Pyx = Ca-pyroxene solid solution; Saph = Mg-Al sapphirine. Components are calculated as follows (oxides are in mole percent): Ca₂SiO₄ = 172.24 (0.5CaO); MgAl₂O₄ = 142.27 (CaO + MgO - 2SiO₂); Mg₂SiO₄ = 140.69 (SiO₂ - 0.5CaO); Al₂O₃ = 101.96 (Al₂O₃ + 2SiO₂ - MgO - CaO). Ternary coordinates for the figure are calculated by dividing each of the three plotted components by their sum (Al₂O₃ + Mg₂SiO₄ + Ca₂SiO₄).

at that point. For example, a chondrule having a spinel coordinate of -80 and plotting near the -100 spinel contour is spinel saturated and would have spinel as its liquidus phase.

In the discussion that follows, we will employ our diagram for two completely different purposes. First, we use it to understand the diverse properties of Al-rich [Oliv] chon-

drules vs. Al-rich [Plag] chondrules vs. Al-rich [Glass] chondrules in the context of phase equilibrium. In this usage, the diagram is strictly valid only for objects that are spinel saturated or slightly undersaturated. However, as will become apparent, the diagram provides considerable insight into the underlying causes of why some objects are spinel saturated and some are not and therefore has utility even for

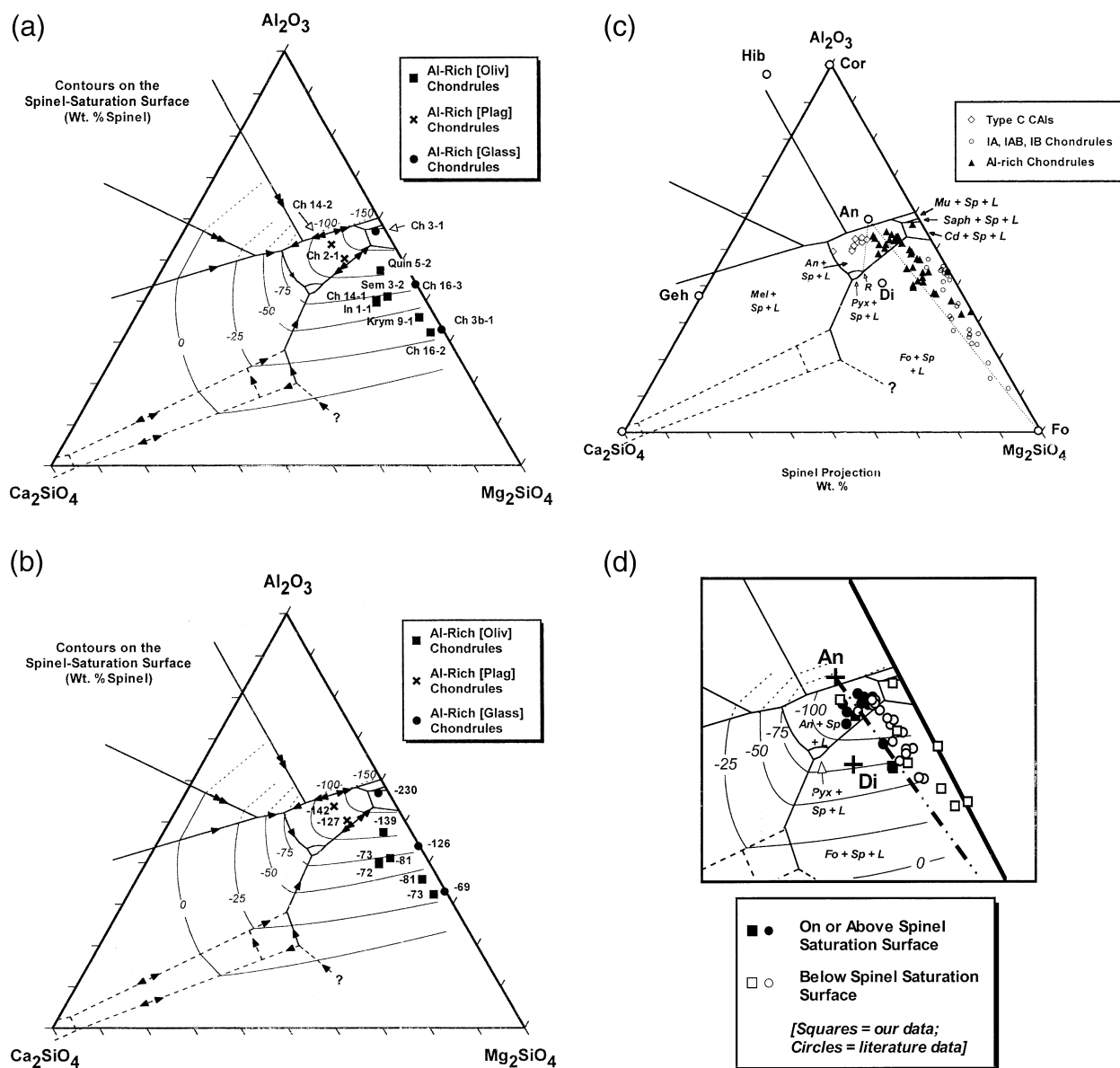


Fig. 9. Bulk compositions of Al-rich chondrules, plotted as in Figure 8. (a, b) The chondrules studied in this work relative to contours on the spinel saturation surface, with their identification (a) and spinel coordinates (b). (c) Our data together with literature data for low-Fe/low-Na Al-rich chondrules (Bischoff and Keil, 1984; Sheng et al., 1991) and, in addition, the compositions of type C CAIs (Wark, 1987). (d) Enlarged view of a portion of (c), showing which Al-rich chondrules compositions plot above the spinel saturation surface and which ones plot below it (see text).

Al-rich chondrules that are significantly spinel undersaturated. Second, we use it to relate the compositions of Al-rich chondrules and CAIs to those of ferromagnesian chondrules. In this usage, the phase relationships do not apply to the latter but neither do they matter; the point is to investigate the compositional relationships between classes of objects and processes that might have produced them.

4.1.1. Phase equilibrium constraints on Al-rich chondrule diversity

Figure 9a and b shows our Al-rich chondrule data only, plotted relative to contours on the spinel saturation surface,

along with their identification (Fig. 9a) and spinel coordinates (Fig. 9b). Figure 9c shows our data together with literature data for a wide diversity of Al-rich chondrules (only ones with <3 wt.% each of FeO and Na_2O are plotted) and for comparison the compositions of type C CAIs (Wark, 1987) and types IA, IAB, and IB ferromagnesian chondrules (Jones and Scott, 1989; Jones, 1994). It is clear from Figure 9c that the Al-rich chondrules define a single coherent trend that straddles the tie line between forsterite and anorthite and crosses the forsterite-anorthite reaction curve. Figure 9d is an enlarged view of Figure 9c showing only data for Al-rich chondrules; it distinguishes between those data points plotting above the spinel

saturation surface from those plotting below it. Between 1/4 and 1/3 of the chondrules (including three of our own) plot above the spinel saturation surface and the rest plot below it. Note also that the vast majority of the Al-rich chondrules plotting below the spinel saturation surface lie to the right of the anorthite-forsterite tie line, whereas most (not all) of the chondrules plotting above the spinel saturation surface lie to the left of the tie line. Clearly the tie line on this spinel-saturated diagram has relevance even to those chondrules that are not spinel saturated; we return to this important point below.

Consider first those chondrules that are spinel saturated or close to it, for which the phase relationships in Figure 9 are valid. The phase relationships of these chondrules are controlled by two boundaries, the anorthite-forsterite (+ spinel) reaction curve and a thermal divide represented by the tie line between anorthite and forsterite (see Fig. 8b). Because of these two boundaries, the chondrules fall naturally into four different groups that evolve differently during crystallization and end up with different mineralogies and textures. The effect of primary phase volume is the more important of the two, because the first crystallizing phase will heavily influence (if not control) the final texture. Those Al-rich chondrules plotting within the forsterite phase volume are expected to have forsterite + spinel as the first crystallizing (phenocryst) phases, whereas those plotting in the anorthite phase volume will instead have anorthite + spinel as the earliest phases. The effect of the thermal divide is more subtle because in general it controls the later stages of melt evolution. Closed-system igneous crystallization of any specific melt composition cannot cross a thermal divide. As different Al-rich chondrule melts evolve during crystallization toward the forsterite-anorthite reaction curve (directly away from either anorthite or forsterite, depending on which primary phase field they plot in), their liquid line of descent will be determined by which side of the thermal divide their bulk compositions lie on. Those hitting the reaction curve on the Ca_2SiO_4 -rich side of the thermal divide will progress toward the calcium-rich pyroxene phase field whereas those hitting the reaction curve on the Ca_2SiO_4 -poor side of the thermal divide will progress in the opposite direction, away from the calcium-rich pyroxene phase field. One can also think of this issue as a matter of geometry: If a melt crystallizes olivine and plagioclase together, the residual composition must evolve away from the tie line joining the two phases (in effect this is a definition of a thermal divide because if it were not true the system on one side or the other would have to crystallize impossibly up-temperature).

The presence of sodium and iron in the natural chondrule melts affects the above discussion in two ways. Both components affect the position of the tie line, and thus the thermal divide, on Figures 8 and 9 because (as noted earlier for Fig. 2) sodium-bearing plagioclase and iron-bearing olivine do not plot at the same positions as anorthite and forsterite. Pure albite plots very close to the position of cordierite (see Fig. 9c), and iron-bearing olivine plots progressively up the right side of the ternary in the direction of corundum (Fo_{85} plots at $\text{Cor} = 18$ on Fig. 9c). The net effect of both components is to shift the olivine-plagioclase tie line progressively to the right on Figures 8 and 9, but for the compositions of most Al-rich chondrules the effect is sufficiently minor that it does not affect the discussion. Iron has the additional effect of largely eliminating

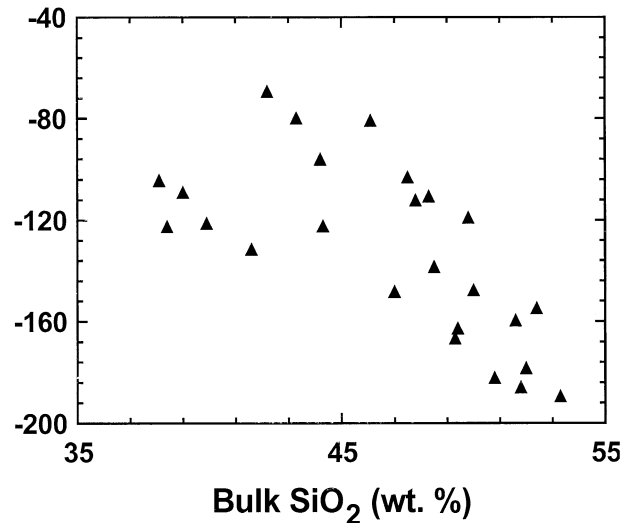


Fig. 10. Correlation between bulk SiO_2 in Al-rich chondrules and spinel coordinate within the system $\text{C}_2\text{S-Fo-Cor}$, showing that silica-enriched chondrules are the most spinel-undersaturated. Only chondrules with $<3\%$ FeO and Na_2O (each) are plotted.

the fields of cordierite, sapphirine, and mullite (Sheng, 1992), which do not appear in any of the chondrules we studied (but see Sheng et al., 1991).

The inferences made above for the spinel-saturated Al-rich chondrules, based on Figure 9, remain remarkably robust for spinel-undersaturated ones as well. For example, the primary phase boundaries on Figure 9 are good indicators of the first crystallizing phase that precedes spinel; this can be verified by plotting the data on diagrams such as those in Figures 2 and 3. All of the spinel-undersaturated Al-rich [Plag] chondrules have anorthite rather than spinel as the first crystallizing phase, as predicted by Figure 9. The spinel-undersaturated Al-rich [Oliv] chondrules are slightly more complex. Although all have forsterite as the first crystallizing phase, as expected, the more silica-rich ones plot sufficiently below the spinel saturation surface that low-calcium pyroxene, rather than spinel, is the second crystallizing phase. This is because these compositions are silica saturated and MgAl_2O_4 spinel is not stable in a silica-saturated melt. This is shown in Figure 10, where the Al-rich chondrule data show an inverse correlation between spinel coordinate (from Fig. 9d) and the bulk SiO_2 wt.% of each chondrule. Turning to the anorthite-forsterite tie line and the thermal divide, most spinel-undersaturated Al-rich chondrules plot to the right of the tie line (Fig. 9), even though the thermal divide as drawn is not strictly relevant to their compositions. In addition, the silica-rich chondrules to the right of the tie line typically contain modal low-calcium pyroxene, a phase generally absent from the spinel-bearing chondrules to the left of the tie line. In short, the primary phase field and the tie line/thermal divide shown on Figure 9 do a good job of predicting the mineralogy of most Al-rich chondrules and not just the spinel-saturated ones.

The basis for the nomenclature system for Al-rich chondrules that we have used throughout this paper now becomes clear. The system is based on composition-dependent textural differences within a coherent larger group (our chondrules, plus

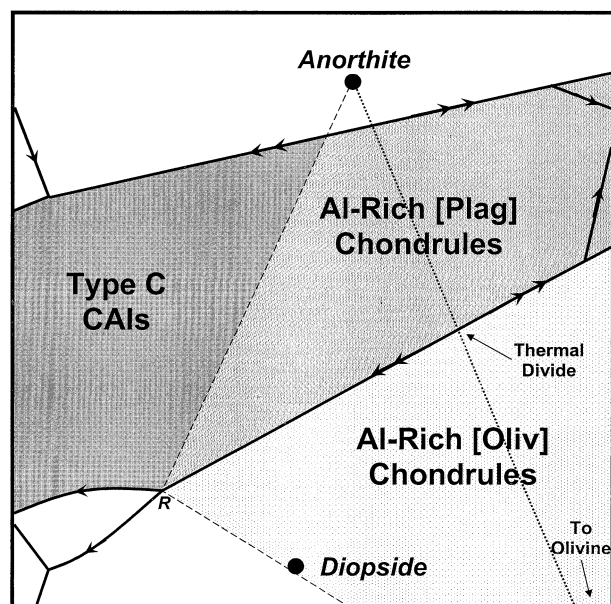


Fig. 11. Proposed nomenclature system for Al-rich chondrules and type C CAIs, based on liquidus relationships in a portion of the system $\text{Ca}_2\text{S-Fo-Cor}$ shown in Figure 8.

literature examples for which sufficient textural information exist), and those textural differences derive largely from the relative crystallization of olivine and plagioclase. The proposed nomenclature system is summarized in Figure 11, which shows an enlarged version of the portion of the phase diagram (Fig. 8) centered on the anorthite-forsterite reaction curve. Those compositions plotting in the forsterite field contain euhedral or barred olivine (\pm spinel) phenocrysts (e.g., Fig. 1a and f), thus the term Al-rich [Oliv] chondrules. These correspond to the group 3 POIs of Sheng et al. (1991). In an analogous fashion, those compositions plotting in the anorthite primary phase volumes ($+$ spinel) have textures dominated by long euhedral plagioclase crystals (e.g., Fig. 1b and c) and interstitial olivine and pyroxene, and therefore are designated as Al-rich [Plag] chondrules; these approximately correspond to the groups 1 and 2 POIs of Sheng et al. (1991). The Al-rich [Plag, Oliv] chondrules collectively are Ca-Al-rich chondrules in the nomenclature of Bischoff and Keil (1984).

The Al-rich [Glass] chondrules (e.g., Fig. 1d) are calcium-poor and sodium-rich and plot on or near the right margin of the ternary (corundum-forsterite side) in Figure 9a. As we will suggest below, they have evolved in a different fashion from their Na-poor and Ca-rich kindred. These Al-rich [Glass] chondrules would have been classified as Na-Al-rich chondrules by Bischoff and Keil (1984).

Note on Figure 9c that type C CAIs occupy a slightly different region than do the Al-rich [Plag] chondrules. They are separated by a line that connects the composition of the mineral anorthite with the ternary reaction point labeled “R” on Figure 9c. Melts of both type C CAI and Al-rich [Plag] chondrule composition are expected to crystallize plagioclase or spinel as their liquidus phase, but the two then evolve very differently precisely because of what the dividing line represents. Type C CAI melts evolve to either the plagioclase-pyroxene cotectic or

the plagioclase-melilite cotectic, and subsequently evolve to the plagioclase-pyroxene-melilite invariant point; they will never crystallize olivine. Al-rich [Plag] chondrules evolve to the olivine-plagioclase reaction curve and then evolve toward the ternary reaction point “R.” At that point plagioclase enters into reaction relationship with the melt and, if it is totally consumed, the melt will then evolve down the olivine-pyroxene cotectic. Thus the tie line between anorthite and the distributary reaction point “R” on Figure 9c provides a meaningful distinction between Al-rich [Plag] chondrules and type C CAIs. Wark (1987) correctly inferred the nature of the difference between the two groups of objects but did not provide the phase equilibrium basis for it: Melts of type C CAI composition will never encounter the forsterite phase field, whereas melts of Al-rich [Plag] chondrule composition always will if they are not quenched beforehand.

4.1.2. Al-rich chondrules, CAIs, and ferromagnesian chondrules: Cosmochemical considerations

Up to now, we have used the ternary diagram in Figures 8 and 9 as a tool for investigating how the properties of diverse Al-rich chondrules can be related to petrologic phase boundaries. Now we turn to using the diagram as a cosmochemical tool for comparing bulk compositions of Al-rich chondrules to those of CAIs and ferromagnesian chondrules. In this context the petrologic phase boundaries are no longer relevant except in a negative sense: The fact that the bulk-composition trends cross-cut the phase boundaries at high angles strongly suggests that igneous processes played no role in governing the bulk compositions of this family of objects.

Figure 12a shows the bulk compositions of Al-rich chondrules (our data, plus data for Al-rich chondrules with low FeO and Na_2O taken from Bischoff and Keil (1984) and Sheng et al. (1991)), a variety of CAIs (Beckett, 1986; Wark, 1987), and types IA, IAB, and IB ferromagnesian chondrules (Jones and Scott, 1989; Jones, 1994) plotted on the $\text{Ca}_2\text{SiO}_4\text{-Fo-Cor}$ diagram. What is striking is that the CAI, Al-rich chondrule, and ferromagnesian chondrule data define a continuous but nonlinear trend. The Al-rich chondrule trend connects the upper end of the CAI trend, which terminates at the anorthite-diopside join, with the ferromagnesian chondrule trend along the right side of the ternary and straddling the bulk solar (CI chondrite) composition. This trend clearly does not correspond in any way to major liquidus boundaries, and thus does not appear to be the result of any igneous processes such as fractional crystallization or fusion. It also is clear from the diagram that although the Al-rich chondrules link the CAI and ferromagnesian chondrule trends, the Al-rich chondrules are not on a mixing line between the ferromagnesian chondrules and any melilite-rich (types A, B) CAIs. Only very anorthite- and diopside-rich CAIs (e.g., type C) could conceivably represent one end of such a mixing line. This conclusion is reinforced in Figure 12b, which shows the same data plotted in approximately a vertical section through the ternary diagram (spinel coordinate of each point plotted vs. the ternary forsterite coordinate). Note on both Figure 12a and b that a mixture of type C CAIs, type IA chondrules, and type IAB/IB chondrules can plausibly account for $\sim 70\%$ of the Al-rich chondrule compositions (the alert reader will perceive that mixing “lines” on this diagram will not

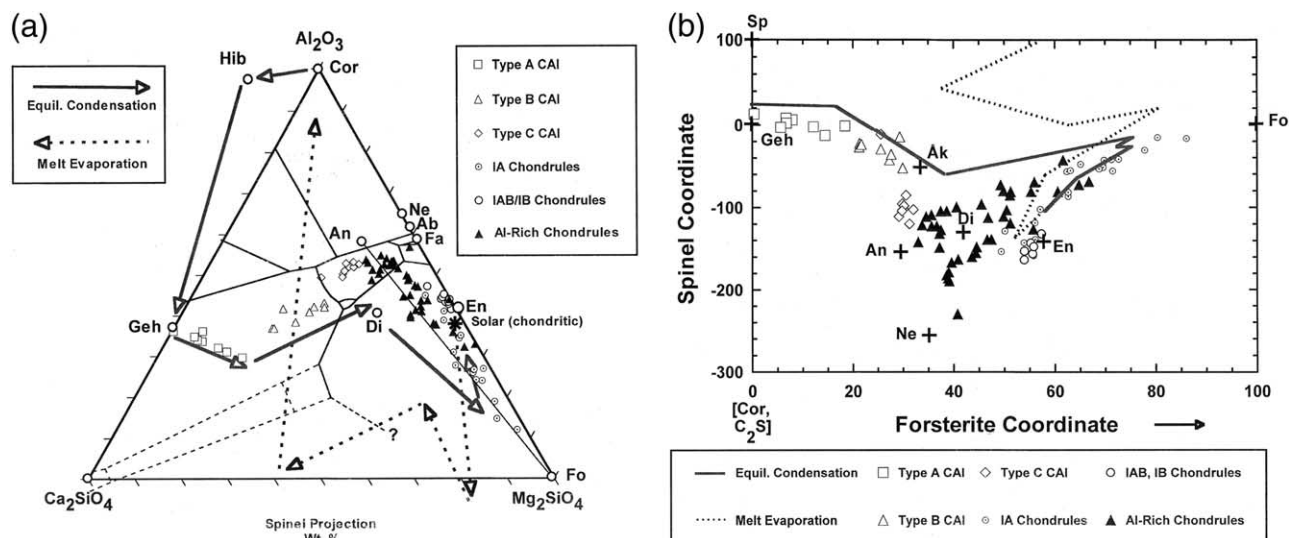


Fig. 12. (a) Bulk compositions of Al-rich chondrules, ferromagnesian chondrules (types IA, IAB, IB), and various kinds of silicate-rich CAIs projected from spinel onto the plane C_2S -Fo-Cor. Data from this study, Beckett (1986), Bischoff and Keil (1984); Sheng et al. (1991), Wark (1987), Weisberg (1987), Jones and Scott (1989), and Jones (1994). The trend for bulk solids during equilibrium condensation of a solar gas is from Yoneda and Grossman, 1995. The trend for melt evaporation residues from a carbonaceous chondrite melt is from Notsu et al. (1978). (b) A “cross section” through (a), plotting the spinel coordinates vs. normative forsterite. The compositions of CAIs, Al-rich chondrules, and ferromagnesian chondrules form a trend that cuts across the phase boundaries and parallels the equilibrium condensation trend. Note that mixing of ferromagnesian chondrules and any type of CAI cannot produce the compositions of the Al-rich chondrules (see text). Note also that, although hibonite apparently lies along an extension of the Al-rich chondrule trajectory in (a), in (b) hibonite plots off the left edge of the diagram at a spinel coordinate of $\sim +21$ and thus cannot be a significant component of Al-rich chondrules.

be strictly linear; however, they are close enough to linear that our arguments remain valid). For the remaining 30%, another component is required, and Figure 12b provides some hints to what the possible component(s) might be: Those points plot below a line joining type C CAIs and types IAB/IB chondrules, extending in the direction of nepheline (shown) or a sodium-bearing plagioclase (albite, not shown, plots at $Sp = -370$, $Fo = 39$).

Also shown in Figure 12 are the trend for residual melts during evaporation of chondritic composition (Notsu et al., 1978) and the predicted composition trend for bulk solids during equilibrium condensation at 10^{-3} atm. nebular pressure (Yoneda and Grossman, 1995). Those two trends differ because equilibrium gas-solid condensation (and sublimation) is controlled by the stoichiometric compositions of the solid phases, whereas the melt evaporation trend is controlled by the continuously varying proportions of evaporating molecular species. The combined chondrule-CAI data collectively define a continuous nonlinear path that parallels, but does not coincide with, that expected from a gas-solid volatility relationship (condensation or sublimation). However, the chondrule-CAI trend does not remotely resemble that defined by chondritic melt evaporation residues. These comparisons suggest that the CAI-chondrule bulk compositions (or those of their precursors) were controlled primarily by vapor-solid rather than vapor-melt processes. Therefore, because Al-rich chondrules link the CAI part of the trend with the ferromagnesian chondrules, they can be considered intermediate between those two groups of objects in the volatility sense, but not in composition.

4.2. Minor and Trace Element Considerations

In the context of the volatility control argument above, the Al-rich chondrule trend in Figure 11 raises the expectation that the abundances of major, minor, and trace refractory elements should increase and volatile elements decrease from the lower right (where ferromagnesian chondrules meet the Al-rich chondrule trend) toward the junction with type C CAIs. For example, the Al-rich [Plag] chondrules and one of the Al-rich [Glass] chondrules, Chainpur 1251-3-1, should have the highest refractory-element contents because they plot closest to the CAI-end of the Al-rich chondrule trend. In fact, these three chondrules do have the highest refractory-element contents of the chondrules studied (Figs. 5–7). Refractory elements in Al-rich [Glass] chondrules increase from Chainpur 5674-3b-1 to Chainpur 1251-16-3 to Chainpur 1251-3-1 (Fig. 7), as expected from Figure 12. And for the most part, refractory elements in Al-rich [Oliv] chondrules increase in the expected sequence (but cf. Quinyambie 6076-5-2 and Inman 5652-1-1, Figs. 5 and 9a). Figure 13 shows these correlations in a different way. Several refractory trace elements plus FeO and Na_2O are plotted vs. the forsterite and Ca_2SiO_4 coordinates from Figure 12a. In essence, the graphs plotted against forsterite show variations of trace elements along the length of the Al-rich chondrule trend in Figure 12a, whereas the graphs plotted against Ca_2SiO_4 show how the same elements vary across the Al-rich chondrule trend (i.e., perpendicular to the corundum-forsterite side of the ternary). The clearest and best correlations exist for the low-FeO Al-rich [Oliv] chondrules (filled squares in Fig. 13) and the Al-rich [Plag] chondrules (open squares in Fig. 13): The

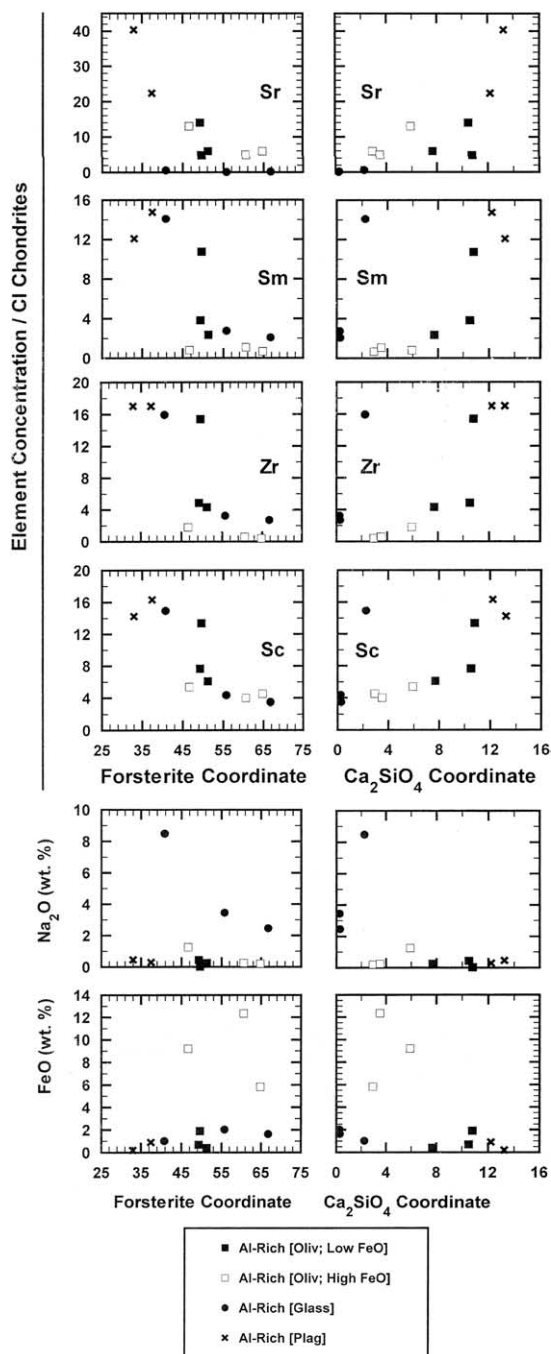


Fig. 13. Abundances of four refractory lithophile trace elements, plus FeO and Na₂O, in Al-rich chondrites plotted both as a function of normative forsterite (left side) and normative Ca₂SiO₄ (right side).

refractory elements generally correlate positively with normative Ca₂SiO₄ and inversely with forsterite; sodium and iron are uniformly low independent of either normative component. The other chondrites fall off these correlations to varying degrees, and the deviations are instructive to examine separately.

The Al-rich [Oliv] chondrites with high FeO (open boxes in Fig. 13) are the three chondrites with the lowest abundances of refractory elements and the most fractionated patterns (Chainpur 1251-16-2, Krymka 1729-9-1, Quinyambie 6075-5-2; Fig.

5). In these chondrites, the calcium, strontium, aluminum, and, in two cases, europium, are enriched relative to the rest of the elements (Fig. 5), suggesting the possible presence of excess plagioclase in the precursor. In Figure 13, the FeO is uniformly high relative to all the other chondrites, with no obvious relationship to either forsterite or Ca₂SiO₄. Thus the iron does not appear to be controlled by volatility. The Al-rich [Glass] chondrites (especially Chainpur 1251-3-1) exhibit two different types of anomalies. First, they are all highly enriched in alkali elements (Fig. 7; Na₂O panels in Fig. 13). Such excesses of highly volatile alkali elements in chondrites that are at the same time both enriched in the refractory elements and depleted in elements of intermediate volatility imply that the alkalis were added later in a secondary process. In addition, the Al-rich [Glass] chondrites also exhibit large negative anomalies in calcium, strontium, and europium (but not aluminum) (Fig. 7). Especially for Chainpur 1251-3-1, its low calcium content shifts it to low Ca₂SiO₄ on Figure 13, yet its refractory-element abundances are comparable to those of chondrites having much higher Ca₂SiO₄, causing it to fall off of the volatility trends. The depleted elements (calcium, strontium, europium) have different volatilities under most conditions, but share in common a tendency to reside in plagioclase. This suggests the depletions are a result of a secondary process that affected the plagioclase component in the chondrites.

4.3. Seeing Through the Fog: Recognizing Secondary Effects

Until the previous paragraph, we have implicitly assumed without evidence that sodium and iron excesses in not only the Al-rich chondrites but also ferromagnesian chondrites are somehow a secondary effect. For example, in selecting the literature data that has been plotted for comparison on various diagrams, only data with less than 3 wt.% each of Na₂O and FeO is used. The assumption has been that such data more clearly reflects the primary processes by which the chondrites were first formed. We are hardly the first to make such an assumption; the idea of secondary processes being responsible for elevated iron and sodium compositions in chondrites has been around for a long time (e.g., Wark 1981; Grossman et al., 1997). We now address this issue for Al-rich chondrites directly. Using the same diagram from Figure 2, we have plotted on Figure 14a the available bulk compositions of Al-rich chondrites and ferromagnesian chondrites, including in both cases those with high FeO and Na₂O contents. The ferromagnesian chondrites show a vague trend away from the tridymite apex, but the Al-rich chondrites scatter widely across the center of the diagram. However, when only those ferromagnesian and Al-rich chondrites containing less than 3 wt.% each of Na₂O and FeO are plotted (Fig. 14b), much of the scatter disappears. The ferromagnesian chondrites define a single coherent trend that extends away from the tridymite apex through bulk solar (CI) toward Al-rich chondrites; the Al-rich chondrites themselves define a relatively tight cluster in the lower central part of the diagram. This observation is significant because addition or subtraction of MgO or SiO₂ (i.e., volatility control) from a solar starting bulk composition will reproduce the trend. Thus, looking at the trends defined by only the FeO- and Na₂O-poor objects apparently reveals the primary compositional variations

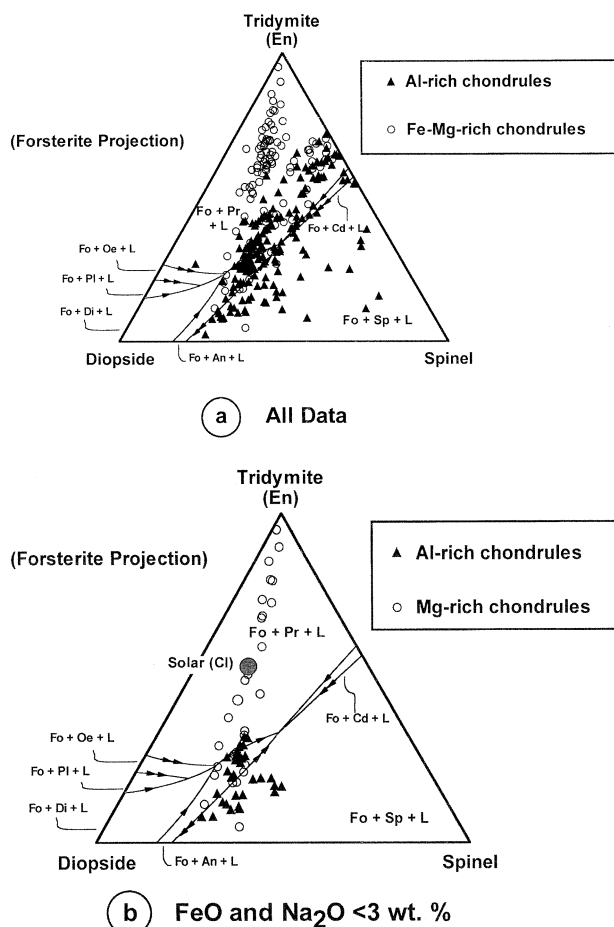


Fig. 14. Bulk compositions of a wide range of ferromagnesian and Al-rich chondrules, including ones enriched in Na_2O and FeO , are projected from forsterite onto the plane tridymite–diopside–spinel. (a) Ferromagnesian chondrules (all kinds, not just type I as in previous figures) show a general trend away from the tridymite apex, but the Al-rich chondrules spread across most of the diagram. (b) When chondrules with more the 3% of either Na_2O or FeO are removed from the diagram, a clearer trend containing both types of chondrules is evident. Data from Bischoff and Keil (1984), Weisberg (1987), Jones and Scott (1989), Jones (1994); Sheng et al. (1991); Huang et al. (1996), and this study. Solar (CI) composition is from Anders and Grevesse (1989).

resulting from volatility processes, whereas the presence of FeO - and Na_2O -rich objects obscures such inferences. For those chondrules in which iron is enriched around grain boundaries or fractures, or where sodium is present as nepheline that replaces plagioclase, it is easy to conclude that those elements are present owing to secondary processes. How then do sodium and iron come to be included as apparently primary components in plagioclase, glass, or olivine in some of our Al-rich chondrules? We suggest that multiple episodes of alteration and remelting are responsible, and we will return to this idea at the end of the paper where a specific and suggestive case can be made for the origin of sodium in the Al-rich [Glass] chondrules.

4.4. The Role of Condensation in the Formation of Al-Rich Chondrule Precursors

We previously noted the clear parallelism between the combined CAI–Al-rich chondrule–ferromagnesian chondrule trend

to that predicted by equilibrium condensation (Section 4.1; Fig. 11), but there is also an inescapable systematic difference between observed and predicted trends. This problem is not new. The systematic deviation of observed CAI compositions (especially types B and C) from the predicted equilibrium condensation trend was discussed at length by Stolper (1982) and Beckett and Grossman (1988). A number of potential reasons for this difference have been proposed. These fall into three categories: The observed compositions are systematically in error, the observed compositions result from additional processes superimposed on the condensation trend, or the existing equilibrium condensation calculations do not accurately reflect the actual nebular condensation.

Grossman et al. (2000) proposed that the bulk compositions for types A and B CAIs may be in error due to nonrepresentative sampling of spinel relative to other phases. When they correct the compositions for this supposed sampling problem, they found better agreement between natural and predicted compositions though significant discrepancies remained.

Grossman et al. (2000, 2002) and Richter et al. (2002) proposed that fractional evaporation during high-temperature cooling of types A and B CAI melts results in preferential loss of magnesium and silicon from the liquids, and they showed how this can explain the discrepancy between calculated and observed CAI compositions. These models are supported by the small degrees of mass-dependent isotopic fractionation of magnesium and silicon that are commonly observed in type B CAIs. These models cannot explain either type C CAIs or Al-rich chondrules, which therefore would necessarily have independent and very different origins from the types A and B CAIs.

The alternative to the above models for explaining the deviation of observed compositions from the calculated condensation trend is that the calculations themselves are in some way inappropriate to the natural situation. For example, Beckett and Grossman (1988) suggested nonequilibrium condensation of anorthite and diopside as a mechanism to explain type C CAIs. MacPherson and Huss (2000) agreed that anorthite is the key: Because condensation calculations generally predict anorthite to condense at a lower temperature than both pyroxene and forsterite, the condensation trend evolves from pyroxene toward forsterite and never approaches anorthite (Fig. 11a). Therefore, MacPherson and Huss (2000) suggested that anorthite preceded forsterite in the actual condensation sequence rather than followed it. This suggestion was based on the observation that, in many CAIs, early-formed phases such as melilite and spinel are replaced by anorthite and pyroxene in the absence of olivine. MacPherson et al. (2002) and Krot et al. (2004a) explored this idea by looking at fine-grained spinel-rich CAIs from Efremovka and Leoville, whose highly fractionated group II trace element patterns are generally considered to establish these CAIs as the best examples of solar nebular condensates. Their mineralogic and textural features demonstrate clearly that anorthite and pyroxene formed as a result of melilite and spinel reacting with the gas, with no intervening forsterite. Thus the observations indicate that anorthite condensation apparently did precede forsterite condensation, at least in the regions where these objects formed. A theoretical study of condensation behavior as a function of nebular pressure (Petaev and Wood, 1998) in fact showed a pressure-dependent crossover of the anorthite–forsterite con-

densation sequence, with anorthite preceding forsterite at the lower pressures. Krot et al. (2004a) refined those preliminary calculations and showed that the crossover occurs at $P_T \leq \sim 10^{-5}$ bars, below which significant anorthite is calculated to condense before forsterite. MacPherson et al. (2004) showed that condensation under such pressures produces a bulk composition trend that is very similar to the one (e.g., Fig. 11a) defined by the CAIs (including type Cs) and Al-rich chondrules.

We have to this point discussed only the possibility of classic vapor–solid condensation. However, Wark (1987) explicitly proposed that type C CAIs might be the result of liquid condensation. Al-rich [Plag] chondrules are similar to type C CAIs in composition, so Wark's proposal (if correct) has obvious relevance. Yoneda and Grossman (1995) and Ebel and Grossman (2000) explored the conditions under which liquid condensation could have occurred in the solar nebula, and what the compositions of such condensates would be. These studies showed that enhanced dust/gas ratios are required to stabilize liquids at acceptable nebular pressures, and that under such suitable conditions it is possible to condense melts that resemble some CAIs and even ferromagnesian chondrules in many respects. However, neither set of calculations produced any compositions that remotely resemble most Al-rich chondrules or Type C CAIs. Based on these results, we rule out melt condensation as a likely model for Al-rich chondrule genesis.

4.5. The Role of Volatilization in the Formation of Al-Rich Chondrule Precursors

An alternative volatility-controlled process that might explain the properties of Al-rich chondrules is volatilization, either melt evaporation or solid sublimation.

The evidence suggests that melt evaporation was not a significant factor in most cases. One of the critical points to emerge from the combined bulk compositional trend of CAIs and Al-rich chondrules on Figure 11 is not just that it approximates the trend of total condensed solids predicted by equilibrium gas–solid condensation calculations, but also that it is so different from that of melt evaporation. As noted earlier, a fundamental difference between the products of equilibrium gas–solid condensation vs. those of melt evaporation is the control in the former case by the stoichiometric compositions of the solid phases, as opposed to evaporation of molecular species from a nonstoichiometric melt. The Al-rich chondrule bulk composition trend lies very nearly on an olivine–plagioclase tie line. A second and possibly less restrictive point is that only one of the eleven chondrules we measured shows evidence of isotopic mass-dependent fractionation in magnesium (Huss et al., 2001), whereas evaporation from a melt droplet sufficient to produce the large enrichments in refractory elements can result in significant enrichment of heavy isotopes in the residual liquid (except under special conditions, such as elevated nebular pressure or elevated gas/dust ratios; e.g., Richter et al., 2002). The one exception is Chainpur 1251-3-1, but evidence given earlier suggests that this fractionated magnesium was inherited from a xenolithic CAI fragment that was incorporated into the chondrule and partially melted. Thus, there is no evidence in the chondrules we studied for significant evaporation from the Al-rich chondrule melts.

In principle, equilibrium sublimation is the reverse of equilibrium gas–solid condensation; in practice there might be differences owing to kinetic influences on both processes. If the solids that are being evaporated consist of minerals other than those predicted by equilibrium condensation, and if kinetic barriers prevent those minerals from being converted to the equilibrium assemblage on a timescale that is short compared to the evaporation time scale, then gas and solid bulk compositions could deviate from those predicted by simply considering equilibrium condensation calculations in reverse. We cannot address this possibility from first principles, nor do our data directly address the issue, but there are compelling arguments that sublimation may have been an important nebular process. For the most part, these are arguments against equilibrium condensation in the classic sense. For condensation to be the dominant process, preexisting solids must have completely (or almost completely) evaporated to provide a gas reservoir from which solids can recondense. Yet many CAIs contain isotopically anomalous calcium, titanium, and other elements that are probably preserved from a site of stellar nucleosynthesis (e.g., Niederer et al., 1980; Niemeyer and Lugmair, 1984; Clayton et al., 1988). Because gases mix very rapidly, eliminating isotope effects, the preservation of isotopic anomalies in the CAIs requires that the precursor solids (presolar grains) were not completely evaporated. The preservation of presolar grains in unmetamorphosed members of all chondrite classes, and correlations between modifications of the complex of presolar grains in each meteorite class and the bulk chemical properties of that class, implies that presolar grains experienced the same thermal processing that produced the meteorite classes (Huss and Lewis, 1995; Huss et al., 2002, 2003). Because much chondrule formation is thought to have postdated this chemical processing (e.g., Grossman and Wasson, 1983), precursors for Al-rich chondrules may well have contained abundant products of thermal processing of presolar dust. However, even if sublimation played a major role in producing chondrule precursors, condensation also played a significant role. For example, the Group II REE pattern can only be produced by condensation from a gas from which the ultrarefractory component is missing (Boynton, 1975; Davis and Grossman, 1979). Reactions between preexisting solids and gas while temperatures drop are in fact condensation reactions. The nephelization of anorthite in some Al-rich chondrule precursors falls into this category. Some ^{16}O -rich signatures in CAIs and chondrules may reflect local condensation from a ^{16}O -rich gas (e.g., Scott and Krot, 2001).

The relative importance of condensation and sublimation will not be settled here. However, there is good evidence that Al-rich chondrules (or their precursors) owe their compositions to volatility-controlled processes, and that condensation of liquid chondrules and evaporation of the chondrule melt droplets were likely not important factors in producing these compositions.

4.6. Al-Rich Chondrules as CAI–Ferromagnesian Chondrule Hybrids

Previous workers have described objects in chondrites that clearly consist of CAI material trapped within once-molten ferromagnesian chondrule droplets (e.g., Sheng et al., 1991;

Misawa and Fujita, 1994; Maruyama et al., 1999; Krot and Keil, 2002; Krot et al., 2002). These compound objects have bulk compositions similar to some Al-rich chondrules and, had they experienced more complete melting, would have similar mineralogy and textures. Such observations raise the possibility that Al-rich chondrules in general represent CAI–ferromagnesian chondrule hybrids.

Our earlier qualitative discussion based on Figure 12 showed that hybridization models are consistent with the bulk compositions of many Al-rich chondrules but are severely restricted by the requirement that the CAI component must have a very limited, plagioclase- and calcic-pyroxene-rich bulk composition similar to that of type C CAIs (see also discussion by Krot and Keil, 2002). Melilite in particular must be an insignificant component in any precursor CAIs. Figures 12a and b shows that mixtures of type C CAIs and type IA and type IAB/IB chondrules can plausibly explain up to ~70% of the Al-rich chondrule compositions plotted on those diagrams. In an effort to more fully explore this conclusion, we conducted some simple numerical mixing calculations. We deliberately did not use minerals for these calculations; with enough minerals, it would of course be possible to closely match any composition. Rather, we were interested in seeing if observed chondrule and CAI compositions could be combined into reasonable approximations of Al-rich chondrule compositions; that, after all, is the essence of the hybrid model for Al-rich chondrules. We simplified our calculations by neglecting iron and sodium, and we modeled only major elements because type C CAIs (like all CAIs) have diverse trace element fractionation patterns that are decoupled from their major-element compositions (Wark, 1987). The components we used were an average Semarkona type IA (olivine-rich) chondrule (Jones and Scott, 1989), an average Semarkona type IAB (pyroxene-rich) chondrule (Jones, 1994), and a type C CAI (Beckett, 1986, his TS26F1; see also Wark, 1987). It quickly became apparent, however, that such numerical models add little to the conclusions already stated. The three-component mixing models give fits for the CMAS oxides within 30 relative % in most cases, but fare very poorly for some of the chondrules. Notable exceptions are Krymka 1729-9-1 (for which the calculated SiO₂, Al₂O₃, MgO, and CaO are all too high), Chainpur 1251-14-2 (calculated MgO is far too high), and all of the Al-rich [Glass] chondrules. In the latter, the models fail completely because the calculated CaO contents far exceed the observed values.

We also briefly explored mixing models using a different variety of CAI, the fine-grained spinel-rich CAIs from CV3 chondrites such as Efremovka and Leoville, and which are also highly plagioclase enriched (e.g., MacPherson et al., 2002). Mixed with the same ferromagnesian chondrules, these give significantly higher residuals than does the type C CAI because the fine-grained CAIs are more spinel normative than either the Al-rich chondrules or the type C CAIs.

Based on the major elements alone, therefore, some Al-rich chondrules can reasonably be modeled as three-component mixtures of plagioclase-pyroxene-rich CAIs plus olivine-rich and pyroxene-rich ferromagnesian chondrules. This result supports suggestions by other workers based on isotopic data (Sheng et al., 1991) and direct observations of hybrid CAI-chondrule objects (Misawa and Fujita, 1994; Krot et al., 2002) that some Al-rich chondrules are the result of melting mixtures

of CAI and ferromagnesian material. However, our calculations also indicate that such mixing models do not work well for all Al-rich chondrules: they fail universally for the Al-rich [Glass] variety, and they also fail for some Al-rich [Oliv] and Al-rich [Plag] as well.

4.6.1. The mystery of the missing melilite

The most serious problem for hybrid models may be the restricted population of CAIs that is required for mixing. Because Al-rich chondrule compositions plot (e.g., Fig. 11) along a line joining ferromagnesian chondrules with anorthite + pyroxene (or anorthite-pyroxene-rich CAIs, such as type Cs) and not along a line joining ferromagnesian chondrules with melilite or melilite-rich CAIs (such as type As), melilite was not a significant component in the precursors to Al-rich chondrules, and only plagioclase and calcic pyroxene (\pm spinel) were. Yet melilite-rich CAIs exist in most types of chondrites and are common in some. If CAI-chondrule hybridization was important in forming the Al-rich chondrule precursors, why was melilite absent when the Al-rich chondrules were forming, and why were only plagioclase-pyroxene-rich CAI materials present? Evidence from short-lived radionuclides (especially ²⁶Al; Kita et al., 2000; Huss et al., 2001) and absolute ages (Amelin et al., 2002) demonstrate that CAIs formed at least 1.5 My before the onset of chondrule formation, so melilite-rich CAIs and fragments certainly existed at the time that the chondrules formed. The only possible conclusion, therefore, is that melilite and melilite-rich CAIs were not volumetrically significant in the *place* where the chondrules formed whereas plagioclase and calcic pyroxene were. This conclusion implies that, in order for hybridization to explain Al-rich chondrules, at some point in time there were two reservoirs of CAI material that became physically separated and followed very different evolutionary paths. The melilite-rich CAIs somehow were removed from the normal evolutionary path that ultimately would have led to most or all of the melilite being replaced by plagioclase and calcic pyroxene. They therefore were missing from the place(s) where Al-rich chondrules ultimately formed, and they only arrived at those places after chondrule formation and just before chondrite accretion. Other CAIs that remained in contact with the nebular gas were mineralogically and chemically transformed into plagioclase-pyroxene-rich varieties. The latter CAIs can be thought of as more fully representing the later stages of condensation, because they have more fully equilibrated with the nebular gas. We can only speculate on what might have happened to the melilite-rich CAIs that allowed them to escape the extensive nebular processing experienced by their plagioclase-pyroxene-rich kin. One possibility is that they alone are the CAIs that experienced bipolar outflow of the kind proposed by Shu et al. (1996), which removed them from the nebular disk and later redeposited them back from the outside. The other CAIs did not become incorporated into the bipolar outflow and thus remained in contact with—and became transformed by—the gas in the nebular disk.

4.7. Amoeboid Olivine Aggregates as Al-Rich Chondrule Precursors

An alternative model is that Al-rich chondrules are not CAI-chondrule hybrids but instead formed by melting of

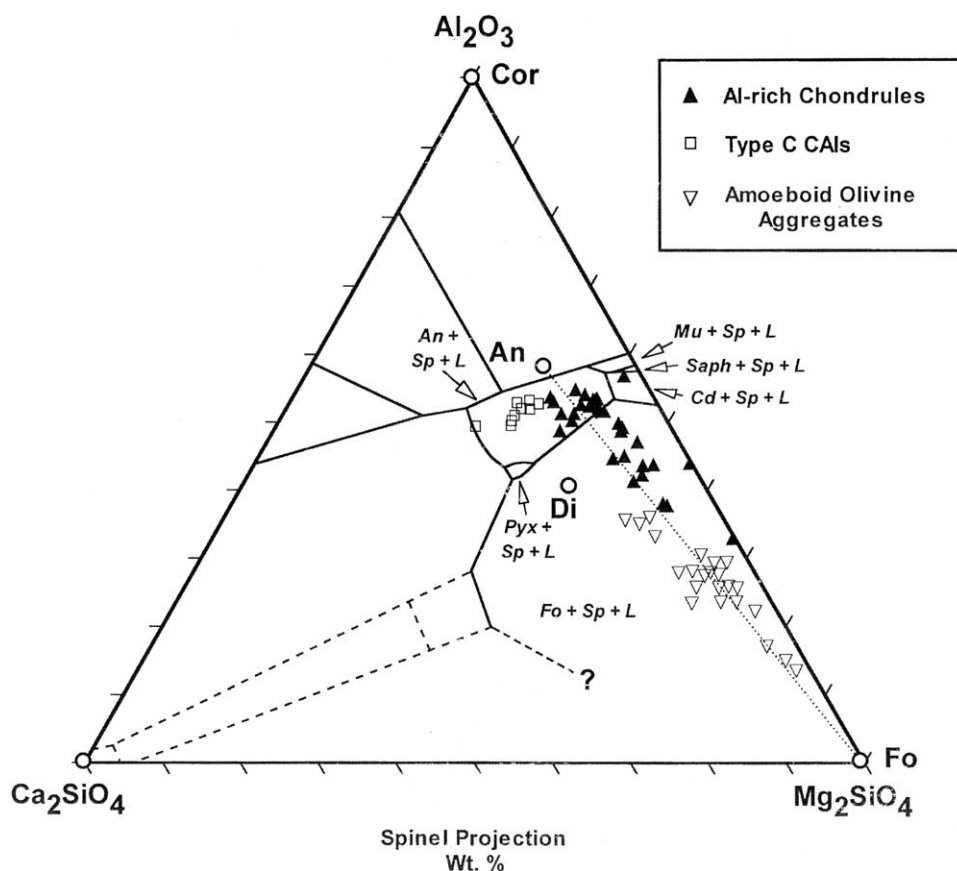


Fig. 15. Compositions of Al-rich chondrules, type C CAIs, and amoeboid olivine aggregates, projected from spinel onto the plane C_2S -Fo-Cor. The AOA data define a trend that is similar to, but more forsterite rich than, that for the Al-rich chondrules. Data from Bischoff and Keil (1984), Wark (1987); Sheng et al. (1991); Komatsu et al. (2001), and this study.

more primitive precursors. In that case it is reasonable to expect that chondrites might contain relicts of those precursors that escaped melting. The critical requirement for such precursors is that they contain abundant olivine together with a refractory component whose modal mineralogy is dominated by calcic plagioclase, calcic pyroxene, and spinel. Objects having such properties are well known from carbonaceous chondrites, and are called amoeboid olivine aggregates (AOAs; see Krot et al., 2004c, for an extensive review). As their name implies, amoeboid olivine aggregates consist largely of olivine (Grossman and Steele, 1976), but most of these large fluffy objects contain within them small refractory nodules composed largely of spinel and pyroxene. The prototypical AOAs, described from Allende, contain abundant nepheline as an additional phase, but recent studies (Komatsu et al., 2001) of AOAs from the reduced CV3 meteorites Leoville and Efremovka show that the nepheline is replacing original anorthite. Very little is known about AOA-like objects from ordinary chondrites, so we necessarily rely on data for ones from CV3s. Figure 15 shows the bulk compositions of AOAs from Efremovka, Leoville, and Vigarano (Komatsu et al., 2001) relative to those of the Al-rich chondrules. The overall bulk chemistry of the AOAs is clearly more olivine-rich than that of the Al-rich chondrules, although they plot along an extension of the same

trend on Figure 15 that leads from forsterite toward anorthite. The overall compositions of the enclosed refractory nodules must be very close to those of the refractory component that went into Al-rich chondrules. Oxygen isotope studies (Hiyagon and Hashimoto, 1999; Clayton et al., 1973; 1977) show that AOAs are distinctly ^{16}O -rich relative to most Al-rich chondrules both in carbonaceous chondrites (Clayton et al., 1987; Maruyama et al., 1999) and in ordinary chondrites (Russell et al., 2000). Komatsu et al. (2001) used similar comparisons to conclude, as do we, that AOAs are intriguingly similar to, but nevertheless not a perfect match for, Al-rich chondrule precursors. It may be that AOAs and Al-rich chondrules both formed from similar yet unidentified precursor materials and then diverged in chemistry during their subsequent different evolutionary paths.

4.8. The Separate Origin of Al-Rich [Glass] Chondrules

The idea that CAIs and chondrules have undergone multiple melting episodes has been around for some time (e.g., MacPherson and Davis, 1993; Jones, 1996; Beckett et al., 2000). Here we suggest how remelting of plagioclase-rich chondrules in which the plagioclase has been altered to nepheline might explain the characteristics of Al-rich [Glass] chondrules. The striking and consistent features of the three Al-rich

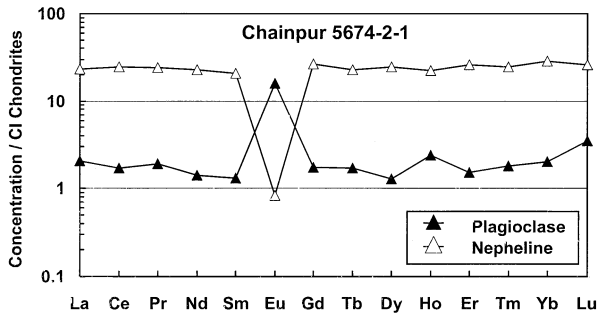


Fig. 16. CI-normalized REE abundances (ion probe data) in plagioclase and nepheline from the Al-rich [Plag] chondrule Chainpur 5674-2-1.

[Glass] chondrules we studied are their uniform enrichments (relative to CI) of elements more refractory than beryllium, elevated sodium and potassium contents, and depletions in calcium, strontium, and europium. The latter suggest removal of plagioclase, but there is no evidence from the major-element bulk composition trends described earlier that igneous fractionation is involved. The key comes not from the Al-rich [Glass] chondrules themselves but from the Al-rich [Plag] chondrules, in which plagioclase is moderately replaced by secondary nepheline (e.g., Fig. 1b). Nepheline is sodium and potassium rich and calcium poor. Our ion probe analyses show that nepheline and plagioclase have virtually reciprocal REE patterns (e.g., Chainpur 5674-2-1; Fig. 16), with plagioclase showing low overall REE contents and a positive europium anomaly, whereas the nepheline is markedly more enriched in all REE except for a large negative europium anomaly. Remelting of such Al-rich chondrules in which the primary plagioclase was moderately to completely replaced by nepheline, such as in Chainpur 5674-2-1 or Chainpur 1251-14-2, would produce the chemical properties of the Al-rich [Glass] chondrules: They retain the elevated overall refractory element abundances of the original chondrules, but calcium, strontium, and europium are lost (presumably to the vapor at the time of alteration) and sodium and potassium are gained with the breakdown of the plagioclase. Interestingly, the alteration process of plagioclase also involves introduction of REE, because the nepheline is significantly more enriched in all REE (except Eu) than the plagioclase it replaces. Note that our model does not require the original chondrules to have been as plagioclase rich as Chainpur 5674-2-1 or Chainpur 1251-14-2, only that they had modal plagioclase that was replaced by nepheline.

5. SUMMARY AND CONCLUSIONS

We have shown that the diverse mineral assemblages and textures exhibited by Al-rich chondrules are a direct consequence of the phase-equilibrium constraints provided by their bulk compositions. The compositions span the anorthite-forsterite reaction curve, which places the compositions into two primary phase fields, the plagioclase (\pm spinel) and olivine (\pm spinel) fields (Figs. 9 and 11). The first-crystallizing phases naturally divide the Al-rich chondrules into plagioclase phyric and olivine phyric varieties. A thermal divide defined by the

anorthite-forsterite join influences the later evolution of the chondrules.

Major-, minor-, and trace-element bulk compositions of eleven Al-rich chondrules previously measured for ^{26}Al (Huss et al., 2001) demonstrate that they are intermediate in a volatility sense between CAIs and ferromagnesian chondrules. When plotted on a new ternary compositional projection diagram that incorporates more of compositional space than previous diagrams, the CAIs, Al-rich chondrules, and ferromagnesian chondrules define a continuous but nonlinear trend through composition space that closely resembles, but does not exactly match, the trend predicted by equilibrium condensation/sublimation. This strongly suggests that volatility-controlled, gas-solid reactions were the dominant processes in producing their compositions. For those Al-rich chondrules that may have formed by remelting of CAI-ferromagnesian chondrule hybrids, the precursors must have originated through volatility-controlled processes. Refractory trace element abundances in the chondrules correlate positively, and volatile element abundances correlate negatively, with normative refractory mineralogy, conforming to expectations if their ultimate precursors formed by condensation or sublimation. Other processes contributed to the further diversification of Al-rich chondrule compositions. Al-rich [Glass] chondrules require complex multi-stage histories, beginning with back-reactions with nebular gas that converted much of the plagioclase in earlier-generation Al-rich chondrules into nepheline. The objects were subsequently remelted, producing Ca-poor and Na-rich glassy chondrules. Clayton et al., 1988 Deer et al., 1966

Acknowledgments—This paper is dedicated to the memory of Dr. Robert M. Walker, a great scientist, visionary, mentor, and friend. We always greatly enjoyed his love of science and his infectious and playful enthusiasm, and we are each profoundly grateful for the gracious hospitality and stimulating experiences during numerous visits to the “MAC” Center at Washington University. We thank Dr. Sara Russell for her editorial patience and support; also, some of the electron microprobe mineral analyses used to calculate the bulk Al-rich chondrule compositions in this paper came from her earlier work while at the Smithsonian during 1995–1997. Dr. Denton Ebel very kindly helped with the MELTS calculations. We have enjoyed numerous discussions with colleagues Sasha Krot, Laurie Leshin, Kevin McKeeagan, and Sara Russell that greatly clarified our thinking about Al-rich chondrules. Finally, we are very grateful for helpful reviews by Drs. Sasha Krot, Harold Connolly, and (notably) John Beckett whose 31-page single-spaced “treatise” is believed to be the longest review of a paper in *GCA* history; all greatly improved the final manuscript. This work was supported by NASA grants NAG5-8158 (GRH) and NAG5-7396 and NAG5-10468 (both to GJM).

Associate editor: S. S. Russell

REFERENCES

- Amelin Y., Krot A. N., Hutcheon I. D., and Ulyanov A. A. (2002) Lead isotopic ages of chondrules and calcium-aluminum-rich inclusions. *Science* **297**, 1678–1683.
- Anders E. and Grevesse N. (1989) Abundances of the elements: Meteoritic and solar. *Geochim. Cosmochim. Acta* **53**, 197–214.
- Armstrong J. T. (1995) CITZAF—A package of correction programs for the quantitative electron microbeam x-ray-analysis of thick polished materials, thin-films and particles. *Microbeam Analysis* **4**, 177–200.
- Beckett J. R. (1986) *The origin of calcium-aluminum-rich inclusions from carbonaceous chondrites: An experimental study*. Ph.D. Thesis. University of Chicago. 373 pp.

- Beckett J. R. and Grossman L. (1988) The origin of type C inclusions from carbonaceous chondrites. *Earth. Planet. Sci. Lett.* **89**, 1–14.
- Beckett J. R. and Stolper E. (1994) The stability of hibonite, melilite and other aluminous phases in silicate melts: Implications for the origin of hibonite-bearing inclusions from carbonaceous chondrites. *Meteoritics* **29**, 41–65.
- Beckett J. R., Simon S. B., and Stolper E. (2000) The partitioning of Na between melilite and liquid: Part II. Applications to type B inclusions from carbonaceous chondrites. *Geochim. Cosmochim. Acta* **64**, 2519–2534.
- Bence A. E. and Albee A. L. (1968) Empirical correction factors for the electron microanalysis of silicates and oxides. *J. Geol.* **76**, 382–403.
- Bischoff A. and Keil K. (1984) Al-rich objects in ordinary chondrites: Related origin of carbonaceous and ordinary chondrites and their constituents. *Geochim. Cosmochim. Acta* **48**, 693–709.
- Bischoff A., Palme H., and Spettel B. (1989) Al-rich chondrules from the Ybbsitz H4-chondrite—evidence for formation by collision and splashing. *Earth Planet. Sci. Lett.* **93**, 170–180.
- Boynton W. V. (1975) Fractionation in the solar nebula: Condensation of yttrium and the rare earth elements. *Geochim. Cosmochim. Acta* **39**, 569–584.
- Clayton R. N., Grossman L., and Mayeda T. K. (1973) A component of primitive nuclear composition in carbonaceous chondrites. *Science* **182**, 485–488.
- Clayton R. N., Hinton R. W., and Davis A. M. (1988) Isotopic variations in the rock-forming elements in meteorites. *Phil. Trans. R. Soc. Lond.* **A325**, 483–501.
- Clayton R. N., Onuma N., Grossman L., and Mayeda T. K. (1977) Distribution of the pre-solar component in Allende and other carbonaceous chondrites. *Earth Planet. Sci. Lett.* **34**, 209–224.
- Clayton R. N., Mayeda T. K., MacPherson G. J., and Grossman L. (1987) Oxygen and silicon isotopes in inclusions and chondrules from Vigarano. *Lunar Planet. Sci. XVIII*. 185–186 (abstr.).
- Clayton R. N., Hinton R. W., and Davis, A. M. (1988) Isotopic variations in the rock-forming elements in meteorites. *Phil. Trans. R. Soc. Lond.* **A325**, 483–501.
- Connolly H. C., Jr., Huss G. R., and Wasserburg G. J. (2001) On the formation of Fe-Ni metal in Renazzo-like carbonaceous chondrites. *Geochim. Cosmochim. Acta* **65**, 4567–4588.
- Davis A. M. and Grossman L. (1979) Condensation and fractionation of rare earths in the solar nebula. *Geochim. Cosmochim. Acta* **43**, 1611–1632.
- Davis A. M., Hashimoto A., Clayton R. N., and Mayeda T. K. (1995) Isotopic and chemical fractionation during evaporation of CaTiO₃. *Lunar Planet. Sci. XXVI*. 317–318 (abstr.).
- Deer W. A., Howie R. A., and Zussman J. (1966) *An Introduction to Rock Forming Minerals*. 528 pp. John Wiley and Sons.
- Ebel D. S. and Grossman L. (2000) Condensation in dust-enriched systems. *Geochim. Cosmochim. Acta* **64**, 339–366.
- Fahey A. J., Goswami J. N., McKeegan K. D., and Zinner E. K. (1987) ²⁶Al, ²⁴⁴Pu, ⁵⁰Ti, REE and trace element abundances in hibonite grains from CM and CV meteorites. *Geochim. Cosmochim. Acta* **51**, 329–350.
- Floss C., El Goresy A., Zinner E., Kransel G., Rammensee W., and Palme H. (1996) Elemental and isotopic fractionation produced through evaporation of the Allende CV chondrite: Implications for the origin of HAL-type hibonite inclusions. *Geochim. Cosmochim. Acta* **60**, 1975–1997.
- Ghiorso M. S. (1985) Chemical mass transfer in magmatic processes I. Thermodynamic relations and numerical algorithms. *Contrib. Mineral. Petrol.* **90**, 107–120.
- Ghiorso M. S. and Sack R. O. (1995) Chemical mass transfer in magmatic processes IV. A revised and internally consistent thermodynamic model for the interpolation and extrapolation of liquid-solid equilibria in magmatic systems at elevated temperatures and pressures. *Contrib. Mineral. Petrol.* **119**, 197–212.
- Grossman J. N. and Wasson J. T. (1983) Refractory precursor components of Semarkona chondrules and the fractionation of refractory elements among chondrites. *Geochim. Cosmochim. Acta* **47**, 759–771.
- Grossman J. N., Rubin A. E., Nagahara H. and King E. A. (1988) Properties of chondrules. In *Meteorites and the Early Solar System* (eds. J. F. Kerridge and M. S. Mathews), pp. 619–659. Univ. Arizona Press.
- Grossman J. N., Alexander C. M. O'D., and Wang J. (1997) Chemical alteration of chondrules on parent bodies. In *Workshop on Parent-Body and Nebular Modification of Chondritic Material*. LPI Technical Report Number 97-02, 19-20.
- Grossman L. and Steele I. M. (1976) Amoeboid olivine aggregates in the Allende meteorite. *Geochim. Cosmochim. Acta* **40**, 149–155.
- Grossman L., Ebel D. S., Simon S. B., Davis A. M., Richter F. M., and Parsad N. M. (2000) Major element chemical and isotopic compositions of refractory inclusions in C3 chondrites: The separate roles of condensation and evaporation. *Geochim. Cosmochim. Acta* **64**, 2879–2894.
- Grossman L., Ebel D. S., and Simon S. B. (2002) Formation of refractory inclusions by evaporation of condensate precursors. *Geochim. Cosmochim. Acta* **66**, 145–161.
- Hiyagon H. and Hashimoto A. (1999) ¹⁶O excesses in olivine inclusions in Yamato-86009 and Murchison Chondrites and their relation to CAIs. *Science* **283**, 828–831.
- Huang S., Lu J., Prinz M., Weisberg M., Benoit P., and Sears D. W. G. (1996) Chondrules: Their diversity and the role of open-system processes during their formation. *Icarus* **122**, 316–346.
- Huss G. R. and Lewis R. S. (1995) Presolar diamond, SiC and graphite in primitive chondrites: Abundances as a function of meteorite class and petrologic type. *Geochim. Cosmochim. Acta* **59**, 115–160.
- Huss G. R., Wasserburg G. J., Russell S. S., and MacPherson G. J. (1997) Trace-element abundances and the origin of aluminum-26-bearing chondrules in unequilibrated ordinary chondrites. *Meteorit. Planet. Sci.* **32**, A63 (abstr.).
- Huss G. R., MacPherson G. J., Wasserburg G. J., Russell S. S., and Srinivasan G. (2001) Aluminum-26 in calcium-aluminum-rich inclusions and chondrules from unequilibrated ordinary chondrites. *Meteorit. Planet. Sci.* **36**, 975–997.
- Huss G. R., Meshik A. P., Hohenberg C. M., and Smith J. B. (2002) Relationships among chondrite groups as inferred from presolar-grain abundances. *Lunar Planet. Sci. XXXIII*. #1910 (abstr.).
- Huss G. R., Meshik A. P., Smith J. B., and Hohenberg C. M. (2003) Presolar diamond, silicon carbide and graphite in carbonaceous chondrites: Implications for thermal processing in the solar nebula. *Geochim. Cosmochim. Acta* **67**, 4823–4848.
- Jones R. H. (1994) Petrology of FeO-poor, porphyritic pyroxene chondrules in the Semarkona chondrite. *Geochim. Cosmochim. Acta* **58**, 5325–5340.
- Jones R. H. (1996) Relict grains in chondrules: Evidence for recycling. In *Chondrules and the Protoplanetary Disk* (eds. R. Hewins, R. Jones and E. Scott), pp. 163–172. Cambridge Univ. Press.
- Jones R. H. and Scott E. R. D. (1989) Petrology and thermal history of Type IA chondrules in the Semarkona (LL3.0) chondrite. *Proc. 19th Lunar Planet. Sci. Conf.* 523–536.
- Kita N. T., Nagahara H., Togashi S., and Morishita Y. (2000) A short formation period of chondrule formation in the solar nebula: Evidence from ²⁶Al in Semarkona ferromagnesian chondrules. *Geochim. Cosmochim. Acta* **64**, 3913–3922.
- Komatsu M., Krot A. N., Petaev M. I., Ulyanov A. A., Keil K., and Miyamoto M. (2001) Mineralogy and petrography of amoeboid olivine aggregates from the reduced CV3 chondrites Efremovka, Leoville and Vigarano: Products of nebular condensation, accretion and annealing. *Meteorit. Planet. Sci.* **36**, 629–641.
- Krot A. N. and Keil K. (2002) Anorthite-rich chondrules in CR and CH carbonaceous chondrites: Genetic link between Ca-, Al-rich inclusions and ferromagnesian chondrules. *Meteorit. Planet. Sci.* **37**, 91–111.
- Krot A. N., Hutcheon I. D., and Keil K. (2002) Plagioclase-rich chondrules in the reduced CV chondrites: Evidence for complex formation history and genetic links between calcium-aluminum-rich inclusions and ferromagnesian chondrules. *Meteorit. Planet. Sci.* **37**, 155–182.
- Krot A. N., MacPherson G. J., Ulyanov A. A., and Petaev M. I. (2004a) Fine-grained, spinel-rich inclusions from the reduced CV chondrites Efremovka and Leoville: I. Mineralogy, petrology and bulk chemistry. *Meteorit. Planet. Sci.* **39**, 1517–1553.
- Krot A. N., Fagan T. J., Keil K., McKeegan K. D., Sahijpal S., Hutcheon I. D., Petaev M. I., and Yurimoto H. (2004b) Ca-, Al-rich

- inclusions, amoeboid olivine aggregates and Al-rich chondrules from the unique carbonaceous chondrite Acfer 094: I. Mineralogy and petrology. *Geochim. Cosmochim. Acta* **68**, 2167–2184.
- Krot A. N., Petaev M. I., Russell S. S., Itoh S., Fagan T. J., Yurimoto H., Chizmadia L., Weisberg M. K., Komatsu M., Ulyanov A. A., and Keil K. (2004c) Amoeboid olivine aggregates and related objects in carbonaceous chondrites: Records of nebular and asteroid processes. *Chemie der Erde* **64**, 185–239.
- Longhi J. and Pan V. (1988) A reconnaissance study of phase boundaries in low-alkali basaltic liquids. *J. Petrol.* **29**, 115–147.
- Longhi J., Walker D., and Hays J. F. (1976) Fe and Mg in plagioclase. *Proc. 7th Lunar Sci. Conf.* 1281–1300.
- MacPherson G. J. and Davis A. M. (1993) A petrologic and ion microprobe study of a Vigarano Type B refractory inclusion: Evolution by multiple stages of alteration and melting. *Geochim. Cosmochim. Acta* **57**, 231–243.
- MacPherson G. J. and Russell S. S. (1997) Origin of aluminum-rich chondrules: constraints from major-element chemistry. *Meteorit. Planet. Sci.* **32**, A83 (abstr.).
- MacPherson G. J. and Huss G. R. (2000) Convergent evolution of CAIs and chondrules: evidence from bulk compositions and a cosmochemical phase diagram. *Lunar Planet. Sci. XXXI*. #1796 (abstr.).
- MacPherson G. J., Krot A. N., Ulyanov A. A., and Hicks T. (2002) A comprehensive study of pristine, fine-grained, spinel-rich inclusions from the Leoville and Efremovka CV3 Chondrites, I: Petrology. *Lunar Planet. Sci. XXXIII*. #1526 (abstr.).
- MacPherson G. J., Petaev M., and Krot A. N. (2004) Bulk compositions of CAIs and Al-rich chondrules: Implications of the reversal of the anorthite / forsterite condensation sequence at low nebular pressures. *Lunar Planet. Sci. XXXV*. # 1838 (abstr.).
- Maruyama S., Yurimoto H., and Sueno S. (1999) Oxygen isotope evidence regarding the formation of spinel-bearing chondrules. *Earth Planet. Sci. Lett.* **169**, 165–171.
- McCoy T. J., Pun A., and Keil K. (1991) Spinel-bearing, Al-rich chondrules: Modified by metamorphism or unchanged since crystallization? *Meteoritics* **26**, 369–370.
- Misawa K. and Fujita T. (1994) A relict refractory inclusion in a ferromagnesian chondrule from the Allende meteorite. *Nature* **368**, 723–726.
- Nagahara H. and Kushiro I. (1982) Calcium-aluminum-rich chondrules in the unequilibrated ordinary chondrites. *Meteoritics* **17**, 55–63.
- Niederer F. R., Papanastassiou D. A., and Wasserburg G. J. (1980) Endemic isotopic anomalies in titanium. *Astrophys. J.* **240**, L73–L77.
- Niemeyer S. and Lugmair G. W. (1984) Titanium isotopic anomalies in meteorites. *Geochim. Cosmochim. Acta* **48**, 1401–1416.
- Notsu K., Onuma N., Nishida N., and Nagasawa H. (1978) High-temperature heating of Allende meteorite. *Geochim. Cosmochim. Acta* **42**, 903–907.
- Petaev M. I. and Wood J. A. (1998) The CWPI model of nebular condensation: Effects of pressure on the condensation sequence. *Meteorit. Planet. Sci.* **33**, A122 (abstr.).
- Prince A. T. (1951) Phase equilibrium relationships in a portion of the system MgO-Al₂O₃-2CaO-SiO₂. *J. Am. Ceram. Soc.* **34**, 44–51.
- Osborne E. F., Gee K. H., Muan A., Roeder P. L., and Ulmer G. C. (1969) Phase equilibria in the systems CaO-MgO- Al₂O₃-SiO₂ and CaO-MgO- Al₂O₃-TiO₂-SiO₂. *Bull. Earth Mineral. Sci. Station, Penn. State Univ.* 85.
- Rao M. R. (1968) Liquidus relations in the quaternary subsystem CaAl₂O₄-CaAl₄O₇-Ca₂Al₂SiO₇-MgAl₂O₄. *J. Am. Ceram. Soc.* **51**, 50–54.
- Richter F. M., Davis A. M., Ebel D. S., and Hashimoto A. (2002) Elemental and isotopic fractionation of type B calcium, aluminum-rich inclusions: Experiments, theoretical considerations and constraints on their thermal evolution. *Geochim. Cosmochim. Acta* **66**, 521–540.
- Russell S. S., Srinivasan G., Huss G. R., Wasserburg G. J., and MacPherson G. J. (1996) Evidence for widespread ²⁶Al in the solar nebula and new constraints for nebula timescales. *Science* **273**, 757–762.
- Russell S. S., Leshin L. A., McKeegan K. D., and MacPherson G. J. (1997a) Oxygen isotope composition of aluminum-rich chondrules: Clues to their origins. *Meteorit. Planet. Sci.* **32**, A111–A112 (abstr.).
- Russell S. S., Huss G. R., MacPherson G. J., and Wasserburg G. J. (1997b) Early and late chondrule formation: New constraints for solar nebula chronology from ²⁶Al/²⁷Al in unequilibrated ordinary chondrites. *Lunar Planet. Sci. XXVIII*. 1209–1210 (abstr.).
- Russell S. S., Leshin L. A., McKeegan K. D., and MacPherson G. J. (1998) Oxygen-16 enrichments in aluminum-rich chondrules from unequilibrated ordinary chondrites. *Lunar Planet. Sci. XXIX*. 1826–1826 (abstr.).
- Russell S. S., MacPherson G. J., Leshin L. A., and McKeegan K. D. (2000) ¹⁶O enrichments in aluminum-rich chondrules from ordinary chondrites. *Earth Planet. Sci. Lett.* **184**, 57–74.
- Scott E. R. D. and Krot A. N. (2001) Oxygen isotopic compositions and origins of calcium-aluminum-rich inclusions and chondrules. *Meteorit. Planet. Sci.* **36**, 1291–1414.
- Sheng Y. J. (1992) *Origin of plagioclase-olivine inclusions*. Ph. D. Thesis. California Institute of Technology.
- Sheng Y. J., Hutcheon I. D., and Wasserburg G. J. (1991) Origin of plagioclase-olivine inclusions in carbonaceous chondrites. *Geochim. Cosmochim. Acta* **55**, 581–599.
- Shu F. H., Shang H., and Lee T. (1996) Toward an astrophysical theory of chondrites. *Science* **271**, 1545–1552.
- Stolper E. (1982), Crystallization sequences of Ca-Al-rich inclusions from Allende: An experimental study. *Geochim. Cosmochim. Acta* **46**, 2159–2180.
- Wark D. A. (1981) Alteration and metasomatism of Allende Ca-Al-rich materials. *Lunar Planet. Sci. XII*. 1145–1147 (abstr.).
- Wark D. A. (1987) Plagioclase-rich inclusions in carbonaceous chondrite meteorites: Liquid condensates? *Geochim. Cosmochim. Acta* **51**, 221–242.
- Weisberg M. K. (1987) Barred olivine chondrules in ordinary chondrites. *Proc. 17th Lunar Planet. Sci. Conf. J. Geophys. Res.* **92**, E663–E678.
- Yoneda S. and Grossman L. (1995) Condensation of CaO-MgO-Al₂O₃-SiO₂ liquids from cosmic gases. *Geochim. Cosmochim. Acta* **59**, 3413–3444.
- Zinner E. K. and Crozaz G. (1986) Ion probe determination of the abundances of all the rare earth elements in single mineral grains. In: *Secondary Ion Mass Spectrometry (SIMS V)* (eds. A. Benninghoven et al.). pp. 444–446. Springer-Verlag.